The IRM Quarterly
Fall 2021, Vol. 31 No. 3
ISSN: 2152-1972

Inside...

Practical Magnetism VII: Avoiding common misconceptions in magnetic fabric interpretation

Andrea Biedermann
University of Bern
andrea.biedermann@geo.unibe.ch

Dario Bilardello
Institute for Rock Magnetism
dario@umn.edu

Brief history – empirical relationships.

Magnetic fabrics, and anisotropy of magnetic susceptibility (AMS) in particular, have long been considered a powerful and time-efficient means of investigating petrofabrics, particularly in the absence of a macroscopic fabric that can be investigated with the naked eye (Borradaile & Henry, 1997; Borradaile & Jackson, 2010; Tarling & Hrouda, 1993). Correlations between magnetic and optical analyses show that in many cases the fabrics obtained with either technique are coaxial, yielding the same orientation of foliation and/or lineation (Balsley & Buddington, 1960). However, this is not always the case, warranting the need to better understand the magnetic anisotropy carriers and the physics that govern these fabrics (Biedermann et al., 2018). Secondly, correlations between magnetic anisotropy degree and strain have been observed in some areas (Kligfield et al., 1977), but these relationships are largely affected by mineralogy (Borradaile, 1987; Housen & van der Pluijm, 1990). This again highlights the importance of understanding how different minerals contribute to the overall magnetic fabric. This article aims at demystifying common misconceptions surrounding magnetic fabrics, which can lead to erroneous interpretations, and suggesting strategies for successful magnetic anisotropy studies.

Sources of magnetic anisotropy.

There are three fundamentally different types of magnetic anisotropy in rocks, depending on the constituent minerals and their occurrence within the bulk rock. The observed magnetic fabric is often a superposition of several contributions.

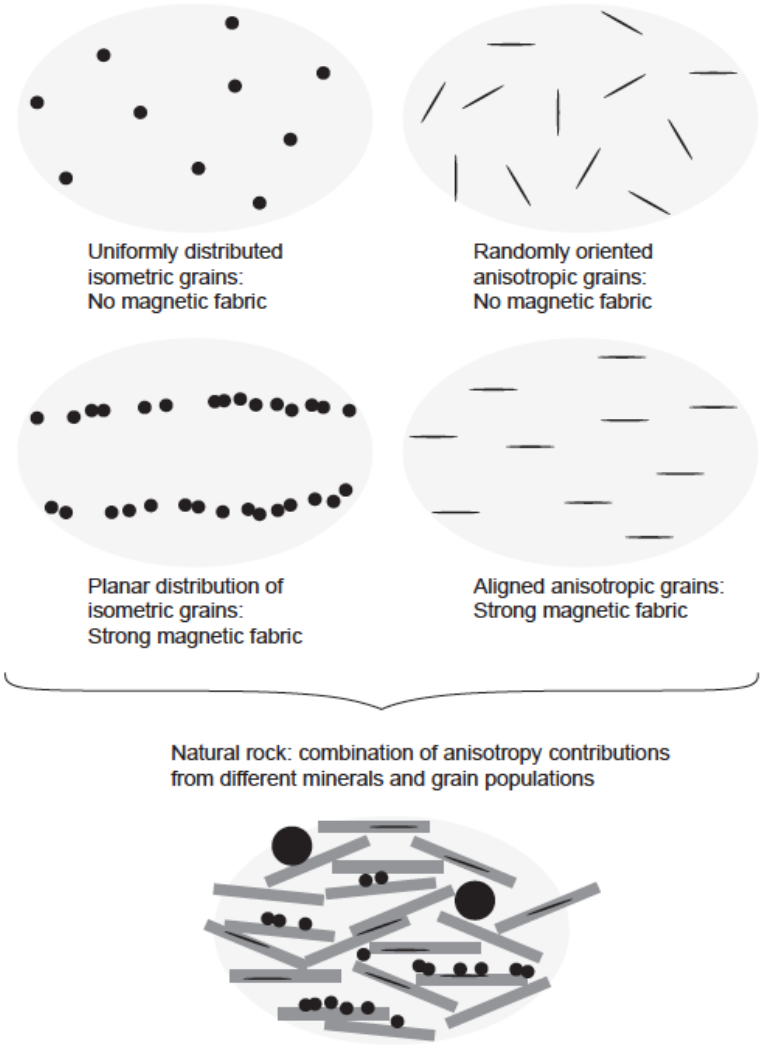

Figure 1: Sketch of the interplay of single crystal/grain properties and alignment or distribution in defining magnetic anisotropy. Note that the degree of alignment shown here is equally important for magnetocrystalline and shape anisotropy. Natural rocks contain a complex assembly of minerals and grain populations (e.g., ferromagnetic and para/diamagnetic grains represented here in black and gray, respectively) and therefore a superposition of anisotropy contributions.

Magnetocrystalline anisotropy occurs in minerals that have their easy and hard magnetization directions controlled by the crystal lattice. It is the dominant source of anisotropy for paramagnetic and diamagnetic minerals, and low-magnetization, but high-coercivity, (parasitic)

cont'd. on pg. 13...

Visiting Fellow Reports

Investigation of strongly negative field-dependence of susceptibility in the subsurface of northeastern Oklahoma

Matt Hamilton
University of Oklahoma
matt.hamilton@ou.edu

Field-dependence (a.k.a. amplitude-dependence) of magnetic susceptibility (χ_{HD}) has found use in the characterization of magnetic mineralogy due to the fact that pyrrhotite, hematite, and titanomagnetite may undergo Rayleigh hysteresis even in the low AC fields commonly used for measurements, leading to increased susceptibility at higher applied fields (e.g., Jackson et al., 1998; Hrouda et al., 2006). However, some geological materials instead exhibit a significant negative variation of susceptibility with increasing fields (Hrouda et al., 2006; Chlupáčová et al., 2010), the origin of which remains unexplained and largely uninvestigated.

During a preliminary study of the basement-cover unconformity from the Amoco SHADS 4 drill core in northeastern Oklahoma (Hamilton et al., 2018), negative χ_{HD} behavior was found in the lower clastic sediments and the uppermost weathered and/or altered igneous rocks (composed of trachyte), with some of the sandstones losing more than 10% of their susceptibility over the range of measuring fields (5-700 A/m). It also became apparent that the same rocks have an elevated frequency-dependence of susceptibility (χ_{FD}), a parameter usually associated with ultra-fine-grained magnetic minerals transitioning from superparamagnetic (SP) to stable single-domain behavior (e.g., Worm, 1998). The magnitudes of these parameters show a reasonable correlation (Fig. 1) and are associated with a decrease in bulk susceptibility in the trachyte. The values of χ_{HD} were more negative than any I could find in the literature, and the relationship to χ_{FD} did not seem to have been noted at all. In addition to the SHADS 4, seven other cores were sampled across the area for a study on alteration of the igneous basement (Hamilton et al., 2021). Susceptibility measurements from these other cores identified samples with significant negative field-dependence in all of them. The relationship between χ_{FD} and negative χ_{HD} varies between locations but is broadly similar to that from the SHADS 4 unconformity, and negative χ_{HD} is never found without significant frequency-dependence. In the igneous rocks (comprised of granite and rhyolite), this behavior is most prominent within the uppermost few meters below the unconformity and may also be found around altered fractures in deeper sections of the cores. In sediments, it is present to varying degrees in clastic units immediately overlying basement but is absent in carbonates.

It was clear that this was a problem worth chasing, but I was out of my depth. I reached out to Martin Chadima at AGICO, who was quite interested, and at his

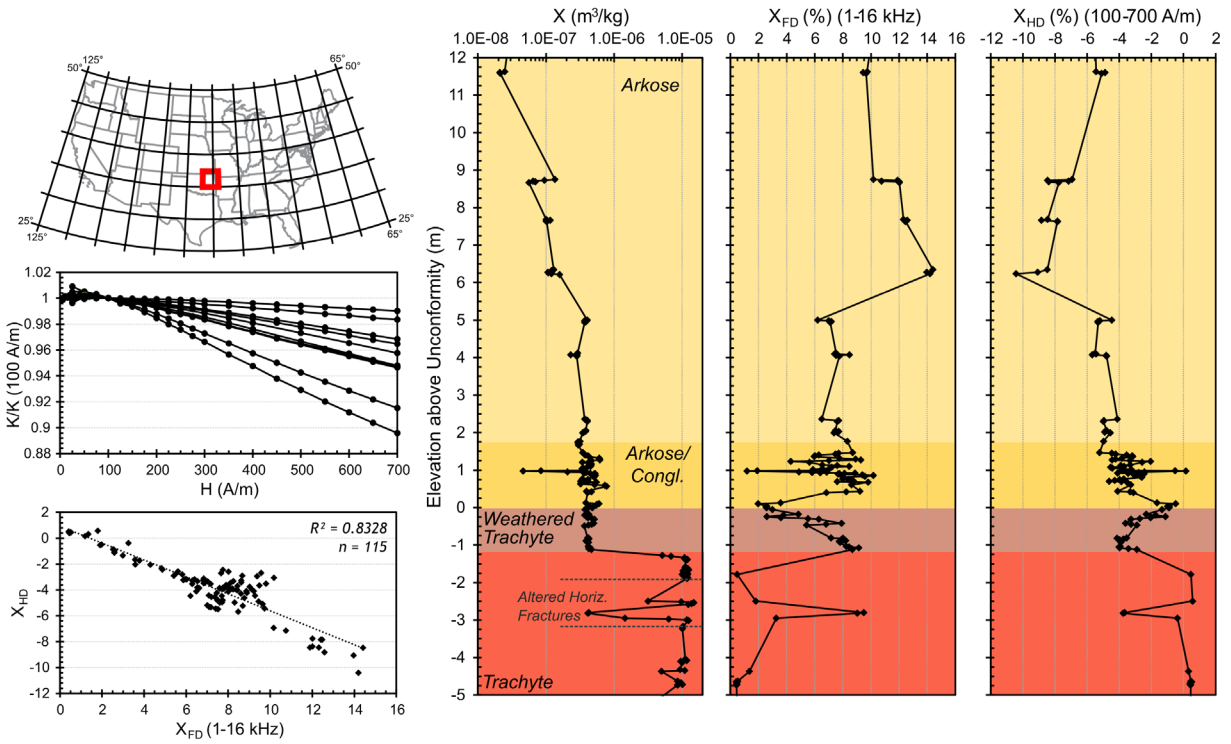

Figure 1. (Left, top) General location of study area. (Left, middle) Representative plots of susceptibility vs. field for samples near the basement unconformity of the Amoco SHADS 4, normalized to the value at 100 A/m. (Left, bottom) Correlation of field-dependence and frequency-dependence of susceptibility for samples from the depth profile. (Right) Depth profile of magnetic susceptibility (200 A/m, 976 Hz), its frequency-dependence and field-dependence across the basement unconformity.

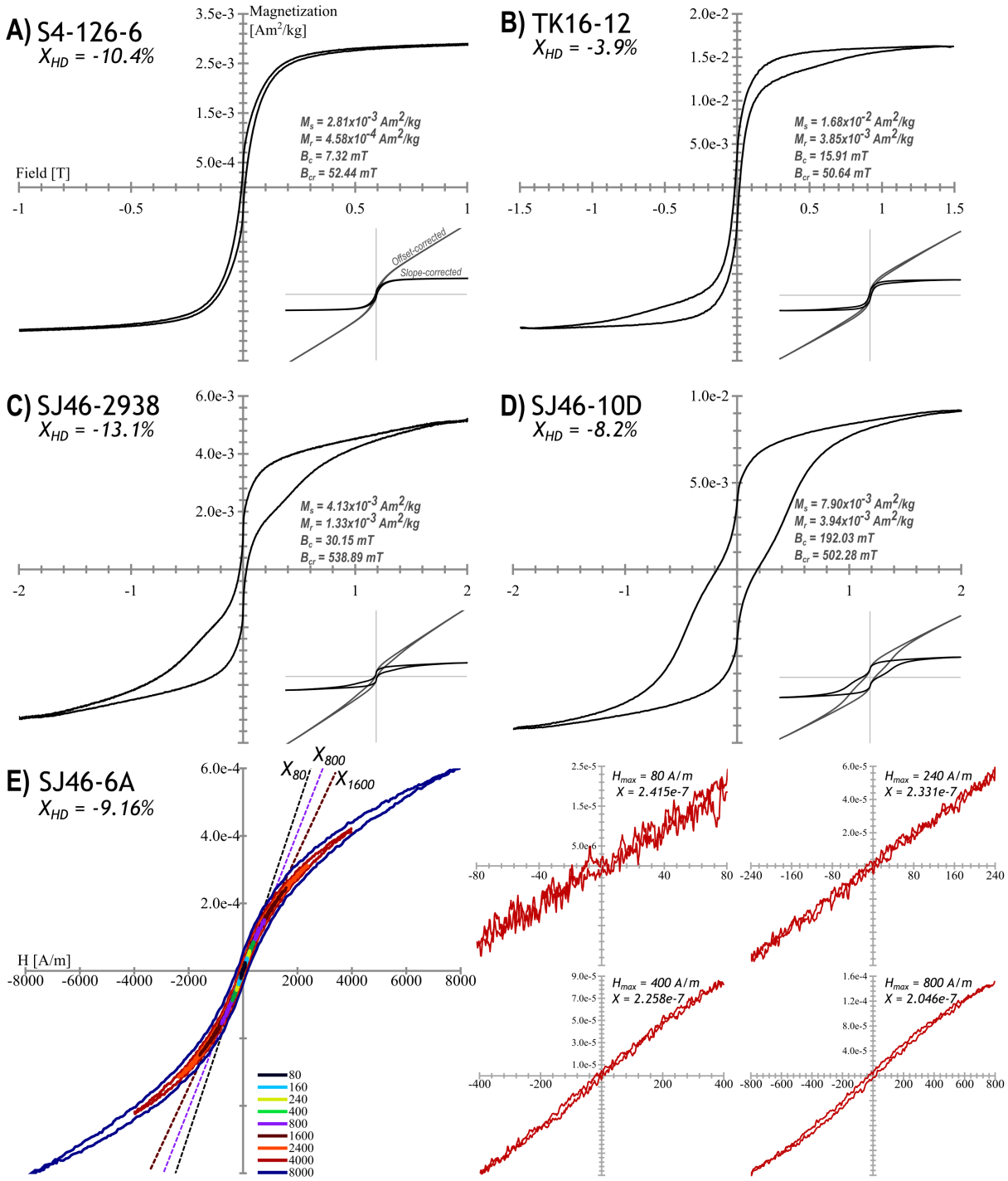

Figure 2. (A-D) Slope-corrected high-field hysteresis loops for specimens from the SHADS 4, Texaco Kohpay 16, and Sinclair Jones 46 cores. Lower-right insets compare loops before and after nonlinear slope-correction (Jackson & Sølheid, 2010). (E) Low-field (≤ 10mT) hysteresis loops for a Jones 46 sample, showing shallowing with increasing field. Individual loops shown on the right, and curvature is visible by H = 1 mT (~800 A/m).

suggestion we also contacted Mike Jackson at the IRM. Mike's theoretical analysis indicated that Langevin behavior of SP magnetite results in negative χ_{HD}, but can only account for a fraction of a percent at the relevant field strengths. Mike made some initial measurements on some samples, and at his invitation I first came to the IRM on an informal visit in November 2019 to collect some additional last-minute data for our AGU presentation (Hamilton et al., 2019). To follow up on those initial data, I returned to the IRM as a visiting fellow in July of 2021 (the first one in-person since the shutdown, they tell me). There were some significant changes from my previous visit – most notably Mike Jackson's retirement and Maxwell Brown's assumption of his post, but also some hardware changes. The new LakeShore VSM (still in its packaging during my first visit) was online, and the "Old Blue" MPMS had been deactivated and replaced with a new MPMS 3.

Due to theoretical constraints, we had suspected that some mineral phase must be approaching saturation at

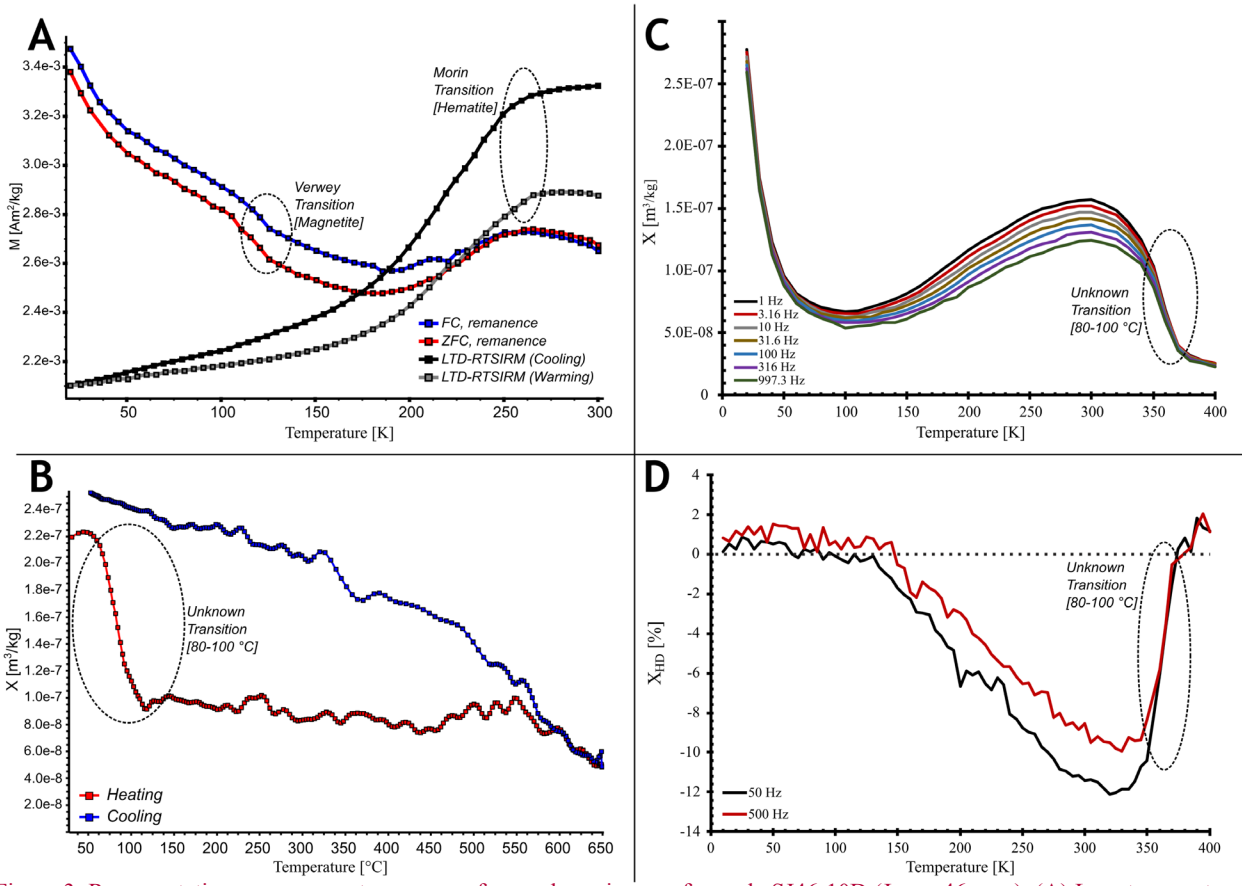

Figure 3. Representative measurement sequences from subspecimens of sample SJ46-10D (Jones 46 core). (A) Low-temperature remanence curves with Morin and very weak Verwey transitions. (B) High-temperature susceptibility with significant loss by 100 °C. (C) χ(f,T) data from 20-400 K showing pronounced frequency-dependence which disappears at the same transition. (D) Field-dependence vs. temperature at 2 frequencies. Negative field-dependence also vanishes in this same temperature range.

very low fields, which is the only sensible physical explanation for this phenomenon that we're aware of. Hysteresis measurements using the VSMs yielded normal to slightly constricted loops with low coercivities for most specimens (e.g., Fig. 2A,B) though some, most notably those from the Sinclair Jones 46 core, have significantly constricted loops with an unusual "pinched-loaf" shape (Fig. 2C,D). Hysteresis measurements with low peak fields also yield shallower slopes (i.e., lower susceptibility values), and by 1 mT many show a curvature which indicates the presence of a phase approaching saturation (Fig. 2E).

During my first visit, we also measured thermal variation of susceptibility using the high-temperature kappabridge and the MPMS systems ("Old Blue" and "Big Red"), as well as remanence curves (e.g., Fig. 3A) using the MPMS. We found little consistency in the remanence curves – most (but not all) specimens exhibited Verwey transitions which ranged from strong to almost invisible, some (but not all) showed the Morin transition of hematite in low-T demagnetization (LTD) of room-T SIRM, and some (but not all) had mildly "hump"-shaped LTD-SIRM cooling curves which are considered an indicator of maghemite (Özdemir and Dunlop, 2010).

Verwey transitions were vanishingly small to absent in low-temperature susceptibility measurements (with the exception of one location). Nearly all specimens instead have very high susceptibility at low T which decreases until reaching a local minimum between 60-100 K, then rises rather smoothly with temperature and reaches a peak near room temperature. Elevated χ_{FD} is present across nearly the entire temperature range. Unusually, the temperature of the susceptibility peak does not appear to vary with frequency despite the significant χ_{FD}.

High-T kappabridge measurements consistently showed significant loss of susceptibility by 100 °C (Fig. 3B), with inspection of $\partial\chi/\partial T$ indicating the strongest slope near 80-85 °C. This change is mostly to completely reversible if peak temperatures do not exceed 200 °C and is completely lost in specimens which exceed 500 °C; these specimens also lose their negative χ_{HD} behavior and often lose most or all of their χ_{FD} as well. The same feature was also seen by pushing "Big Red" to temperatures of 400 K (Fig. 3C), and the prominent frequency-dependence of these specimens is partially to almost completely lost in this same temperature range.

The arrival of the MPMS3 was a fortuitous development for this project. The apparent relationship of negative χ_{HD} with an apparent Curie temperature ~85 °C was an obvious target for study – we suspected that it would diminish or disappear in that range, but setting up a suitable experiment was not a simple endeavor. Mike and I previously attempted to measure χ_{HD} vs. temperature using "Big Red", but the resulting dataset was not useful due to the limited AC field range (H_{max} = 3 Oe, ≈ 240 A/m), and the Kappabridge furnace system could not hold a steady temperature long enough for a χ_{HD} mea-

surement sequence. The MPMS 3 is capable of reaching AC fields of 10 Oe (795.8 A/m) and like Big Red it can measure up to 400 K, making it an ideal candidate for a direct experiment. While it was listed as "Coming Soon!" on the website, Maxwell Brown told me that it was up and running during the IRM conference in June. When he passed the word that in-person visits were opening earlier than expected, I immediately asked for the earliest available time. The χ_{HD} vs. T experiment was the first priority.

My first day, Peat and Dario helped work out and set up a measurement sequence using 1 Oe field increments up to 10 Oe at 50, 158, and 500 Hz (we found out the instrument cannot use its full field range at high frequency) from 10 to 400 K. The control software estimated it would take ~15 hours, so we set it going and looked forward to pulling off the data in the morning. Mike Jackson even came by to check on it the next morning, only for us to discover the sequence was barely a third of the way complete! Peat explained that changing measurement fields takes extra time that the software estimate does not account for (he knew this originally, but we had no idea just how much extra time it would be). We paused and revised the sequence, removing the middle frequency and half the field steps. The measurements finally completed late that afternoon, and I was able to organize the data and calculate χ_{HD} (using linear regression from 1 to 9 Oe, which is very similar to the field range used by the MFK kappabridges) that evening. The results were a bit noisy but very promising – negative χ_{HD} rapidly weakened and disappeared between 360 and 385 K (Fig. 3D). The next morning, I had an email from Martin Chadima – he had been working on a new measurement protocol using AGICO hardware, and his initial tests yielded the same result.

We did run into some noise issues, but after some troubleshooting we were able to obtain more data sets with clean trends which yielded very similar results. Beyond the χ_{HD} vs. T experiments, I also continued to gather χ(f,T) and low-T remanence data using Big Red, thermomagnetic curves from the kappabridge, and hysteresis measurements with the VSMs. I consider this visit as very successful – the new data clearly connects negative χ_{HD} to a frequency-dependent phase with a Curie temperature near 85 °C, and the relationship with fluid alteration suggests that it may have potential as an indicator of specific chemical conditions. Plans for further measurements are in development. In the meantime, there is a lot of work to do with the data so far.

Acknowledgements

I am very grateful to Dario Bilardello and Peter (Peat) Sølheid for their assistance, advice and patience during this visit (and to Mike Jackson as well during my first trip). "Above and beyond" is not an adequate description. I am also grateful to Maxwell Brown for enabling me to make this trip at the earliest possible time, and my advisor (Dr. R.D. Elmore) for encouraging and supporting this work.

References

Chlupáčová, M., Hanák, J. and Müller, P., 2010. Magnetic susceptibility of cambisol profiles in the vicinity of the Vir Dam, Czech Republic. Studia Geophysica et Geodaetica, 54(1), 153-184. doi: 10.1007/s11200-010-0008-8

Hamilton, M., Evans, S.C. and Elmore, R.D., 2018. Magnetic and geochemical characteristics of alteration and weathering at the Cambrian unconformity, northeastern Oklahoma. Abstract GP43C-0788 presented at 2018 AGU Fall Meeting, Washington D.C., 10-14 Dec.

Hamilton, M., Chadima, M., Jackson, M. and Elmore, R.D., 2019. Investigation of Strongly Negative Field-Dependence of AC Magnetic Susceptibility. Abstract GP13A-04 presented at 2019 AGU Fall Meeting, San Francisco CA, 9-13 Dec.

Hamilton, M., Carpenter, B., Johnston, C., Kolawole, F., Evans, S. and Elmore, R.D., 2021. Fractured, altered, and faulted basement in northeastern Oklahoma: Implications for induced seismicity. Journal of Structural Geology, 147, 104330. doi: 10.1016/j.jsg.2021.104330

Hrouda, F., Chlupáčová, M. and Mrázová, S., 2006. Low-field variation of magnetic susceptibility as a tool for magnetic mineralogy of rocks. Physics of the Earth and Planetary Interiors, 154, 323-336. doi: 10.1016/j.pepi.2005.09.013

Jackson, M. and Sølheid, P., 2010. On the quantitative analysis and evaluation of magnetic hysteresis data. Geochemistry, Geophysics, Geosystems, 11(4), Q04Z15. doi: 10.1029/2009GC002932

Jackson, M., Moskowitz, B., Rosenbaum, J. and Kissel, C., 1998. Field-dependence of AC susceptibility in titanomagnetites. Earth and Planetary Science Letters, 157(3-4), 129-139. doi: 10.1016/S0012-821X(98)00032-6

Özdemir, Ö. and Dunlop, D.J., 2010. Hallmarks of maghemitization in low-temperature remanence cycling of partially oxidized magnetite nanoparticles. Journal of Geophysical Research: Solid Earth, 115, B02101. doi: 10.1029/2009JB006756

Worm, H-U., 1998. On the superparamagnetic-stable single domain transition for magnetite, and frequency dependence of susceptibility. Geophysical Journal International, 133, 201-206. doi: 10.1046/j.1365-246X.1998.1331468.x

Want to get better at interpreting anisotropy of physical properties in rocks?

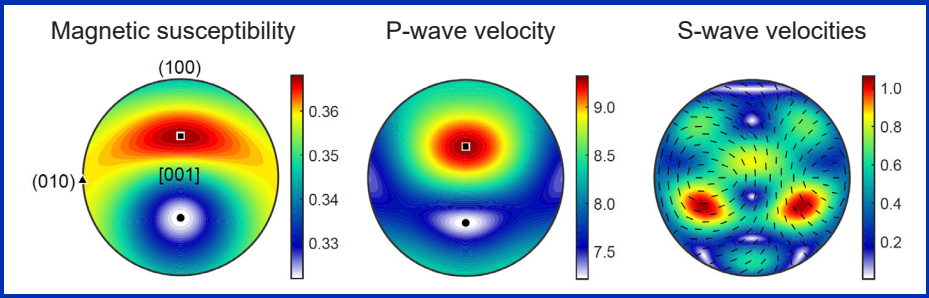

The workshop '***Predicting Anisotropic Physical Properties From Mineralogy and Texture***' on Sunday, 12 December 2021, 8am – 12pm CST will help you to

- understand crystal physical properties and other sources of anisotropy
- use texture and microstructures as a basis to predict anisotropies
- learn how to upscale laboratory measurements to field observations
- develop numerical models to reliably interpret measured anisotropies

We are looking forward to seeing you, on-site or online!

Andrea Biedermann, University of Bern, Switzerland
Bjarne Almqvist, Uppsala University, Sweden
Sarah Brownlee, Wayne State University, USA

Sign up with your AGU Fall Meeting registration

UNIVERSITÄT BERN
UPPSALA UNIVERSITET
WAYNE STATE UNIVERSITY
AGU FALL MEETING
New Orleans, LA & Online Everywhere
13–17 December 2021

Current Articles

A list of current research articles dealing with various topics in the physics and chemistry of magnetism is a regular feature of the IRM Quarterly. Articles published in familiar geology and geophysics journals are included; special emphasis is given to current articles from physics, chemistry, and materials-science journals. Most are taken from ISI Web of Knowledge, after which they are subjected to Procrustean culling for this newsletter. An extensive reference list of articles (primarily about rock magnetism, the physics and chemistry of magnetism, and some paleomagnetism) is continually updated at the IRM. This list, with more than 10,000 references, is available free of charge. Your contributions both to the list and to the Current Articles section of the IRM Quarterly are always welcome.

Archaeomagnetism

Brown, M. C., G. Herve, M. Korte, and A. Genevey (2021), Global archaeomagnetic data: The state of the art and future challenges, Physics of the Earth and Planetary Interiors, 318, doi:10.1016/j.pepi.2021.106766.

Garcia-Garcia, E., H. Grison, N. Jordanova, P. De Smedt, and E. Iriarte (2021), Mineral-Magnetic Characterization as a Key to Explain Differences in Magnetic Contrast and Improve Archaeological Interpretation An Example of the Roman Site at Auritz/Aurizberri, Navarre, Archeosciences-Revue D Archeometrie, 45(1), 161-164, doi:10.4000/archeosciences.9280.

Guiblais-Starck, A., C. Menbrives, S. Coubray, G. Dandurand, A. Giosa, S. Martin, and C. Petit (2020), First archaeological identification of medieval paring and burning: the Vaudes "Les Trappes" site (Aube), Archeosciences-Revue D Archeometrie, 44(2), 219-235, doi:10.4000/archeosciences.7900.

Madingou, B. T., M. Perrin, G. Herve, A. H. Cardona, L. M. Alva-Valdivia, and R. C. Antillon (2021), First Full Vector Archeomagnetic Data From Northern Mexico, Geochemistry Geophysics Geosystems, 22(10), doi:10.1029/2021gc009969.

Environmental Magnetism

Aubourg, C., M. Kars, J. P. Pozzi, M. Mazurek, and O. Grauby (2021), A Magnetic Geothermometer in Moderately Buried Shales, Minerals, 11(9), doi:10.3390/min11090957.

Badejo, S. A., A. R. Muxworthy, A. Fraser, G. R. Stevenson, X. Zhao, and M. Jackson (2021), Identification of magnetic enhancement at hydrocarbon-fluid contacts, Aapg Bulletin, 105(10), 1973-1991, doi:10.1306/07062019207.

Baranov, A., A. Morelli, and A. Chuvaev (2021), ANTASed - An Updated Sediment Model for Antarctica, Frontiers in Earth Science, 9, doi:10.3389/feart.2021.722699.

Bradak, B., G. Ujvari, T. Stevens, M. F. Bogalo, M. I. Gonzalez, M. Hyodo, and C. Gomez (2022), Potential drivers of disparity in early Middle Pleistocene interglacial climate response over Eurasia, Palaeogeography Palaeoclimatology Palaeoecology, 585, doi:10.1016/j.palaeo.2021.110719.

Cai, Y. F., X. Y. Long, X. Q. Meng, J. F. Ji, Y. Wang, and S. Y. Xie (2021), Coordinated and Competitive Formation of Soil Magnetic Particles Driven by Contrary Climate Development, Geophysical Research Letters, 48(16), doi:10.1029/2021gl094506.

Chen, Z. X., S. L. Yang, Y. L. Luo, H. Chen, L. Liu, X. J. Liu, S. Y. Wang, J. H. Yang, W. D. Tian, and D. S. Xia (2022), HIRM variation in the Ganzi loess of the eastern Tibetan Plateau since the last interglacial period and its paleotemperature implications for the source region, Gondwana Research, 101, 233-242, doi:10.1016/j.gr.2021.08.008.

Constantin, D., et al. (2021), OSL-dating of the Pleistocene-Holocene climatic transition in loess from China, Europe and North America, and evidence for accretionary pedogenesis, Earth-Science Reviews, 221, doi:10.1016/j.earscirev.2021.103769.

Danladi, I. B., S. Akcer-On, Z. B. On, and S. Schmidt (2021), High-resolution temperature and precipitation variability of southwest Anatolia since 1730 CE from Lake Golcuk sedimentary records, Turkish Journal of Earth Sciences, 30(5), 601-610, doi:10.3906/yer-2008-14.

Faur, L., et al. (2021), Multi-Proxy Study of a Holocene Soil Profile from Romania and Its Relevance for Speleothem Based Paleoenvironmental Reconstructions, Minerals, 11(8), doi:10.3390/min11080873.

Galli, C. I., R. N. Alonso, E. B. Amoros, H. Pingel, E. Eveling, B. L. Coira, D. F. Stockli, and D. Gonzalez (2021), Plio-Pleistocene paleoenvironmental evolution of the intermontane Humahuaca Basin, southern Central Andes, Journal of South American Earth Sciences, 111, doi:10.1016/j.jsames.2021.103502.

Gao, X. B., Q. Z. Hao, Y. S. Qiao, S. Z. Peng, N. Li, W. Zhang, L. Han, C. L. Deng, S. B. Markovic, and Z. T. Guo (2021), Precipitation thresholds for iron oxides dissolution and the enhanced Eurasian aridity across the Mid-Pleistocene Transition: Evidence from loess deposits in subtropical China, Global and Planetary Change, 204, doi:10.1016/j.gloplacha.2021.103580.

Gokhale, A. A., D. P. Dobhal, and H. C. Nainwal (2021), Source characterization of suspended sediments transported from debris-covered Chorabari Glacier in Central Himalaya, India, Arabian Journal of Geosciences, 14(22), doi:10.1007/s12517-021-08474-5.

Grison, H., E. Petrovsky, and H. Hanzlikova (2021), Assessing anthropogenic contribution in highly magnetic forest soils developed on basalts using magnetic susceptibility and concentration of elements, Catena, 206, doi:10.1016/j.catena.2021.105480.

Hajna, N. Z., et al. (2021), Pliocene to Holocene chronostratigraphy and palaeoenvironmental records from cave sediments: Raciska pecina section (SW Slovenia), Quaternary International, 605, 5-24, doi:10.1016/j.quaint.2021.02.035.

Haskouei, M. F., H. Alimohammadian, and J. Sabouri (2021), magnetic parameters and paleoclimate: a case study of loess deposits of North-East of Iran, Geofisica Internacional, 60(4), 280-293, doi:10.22201/igeof.00167169p.2021.60.4.1949.

Havas, R., J. F. Savian, and V. Busigny (2021), Iron isotope signature of magnetofossils and oceanic biogeochemical changes through the Middle Eocene Climatic Optimum, Geochimica Et Cosmochimica Acta, 311, 332-352, doi:10.1016/j.gca.2021.07.007.

Jia, Y. N., et al. (2022), Late Pleistocene-Holocene aeolian loess-paleosol sections in the Yellow River source area on the northeast Tibetan Plateau: chronostratigraphy, sediment provenance, and implications for paleoclimate reconstruction, Catena, 208, doi:10.1016/j.catena.2021.105777.

Jiang, X. D., X. Y. Zhao, X. Zhao, Z. X. Jiang, Y. M. Chou, T. W. Zhang, X. Q. Yang, and Q. S. Liu (2021), Quantifying Contributions of Magnetic Inclusions Within Silicates to Marine Sediments: A Dissolution Approach to Isolating Volcanic Signals for Improved Paleoenvironmental Reconstruction, Journal of Geophysical Research-Solid Earth, 126(10), doi:10.1029/2021jb022680.

Johnson, J. E., S. C. Phillips, W. C. Clyde, L. Giosan, and M.

E. Torres (2021), Isolating Detrital and Diagenetic Signals in Magnetic Susceptibility Records From Methane-Bearing Marine Sediments, Geochemistry Geophysics Geosystems, 22(9), doi:10.1029/2021gc009867.

Joshi, A. U., and M. A. Limaye (2020), Anisotropy of Magnetic Susceptibility (AMS) Studies on Quartzites of Champaner Group, Upper Aravallis: An Implication to Decode Regional Tectonics of Southern Aravalli Mountain Belt (SAMB), Gujarat, Western India, in Structural Geometry of Mobile Belts of the Indian Subcontinent, edited by T. K. Biswal, S. K. Ray and B. Grasemann, pp. 199-211, doi:10.1007/978-3-030-40593-9_9.

Kars, M., M. Koster, S. Henkel, R. Stein, F. Schubotz, X. Zhao, S. A. Bowden, A. P. Roberts, and K. Kodama (2021), Influence of Early Low-Temperature and Later High-Temperature Diagenesis on Magnetic Mineral Assemblages in Marine Sediments From the Nankai Trough, Geochemistry Geophysics Geosystems, 22(10), doi:10.1029/2021gc010133.

Khatri, D. B., W. L. Zhang, X. M. Fang, Q. Q. Meng, T. Zhang, D. W. Zhang, and K. N. Paudayal (2021), Rock Magnetism of Late Cretaceous to Middle Eocene Strata in the Lesser Himalaya, Western Nepal: Inferences Regarding the Paleoenvironment, Frontiers in Earth Science, 9, doi:10.3389/feart.2021.744063.

Koltringer, C., T. Stevens, B. Bradak, B. Almqvist, R. Kurbanov, I. Snowball, and S. Yarovaya (2021), Enviromagnetic study of Late Quaternary environmental evolution in Lower Volga loess sequences, Russia, Quaternary Research, 103, 49-73, doi:10.1017/qua.2020.73.

Leite, E. C. P., F. M. Rodrigues, T. S. T. Horimouti, M. C. Shinzato, C. R. Nakayama, and J. G. de Freitas (2021), Thermally-induced changes in tropical soils properties and potential implications to sequential nature-based solutions, Journal of Contaminant Hydrology, 241, doi:10.1016/j.jconhyd.2021.103808.

Lu, Y., D. F. Wang, X. D. Jiang, Z. Y. Lin, Y. P. Yang, and Q. S. Liu (2021), Paleoenvironmental Significance of Magnetofossils in Pelagic Sediments in the Equatorial Pacific Ocean Before and After the Eocene/Oligocene Boundary, Journal of Geophysical Research-Solid Earth, 126(9), doi:10.1029/2021jb022221.

Makwana, N., S. P. Prizomwala, A. Das, B. Phartiyal, A. Sodhi, and C. Vedpathak (2021), Reconstructing the Climate Variability During the Last 5000 Years From the Banni Plains, Kachchh, Western India, Frontiers in Earth Science, 9, doi:10.3389/feart.2021.679689.

Munoz-Salinas, E., M. Castillo, F. Romero, and A. Correa-Metrio (2021), Understanding sedimentation at the El Molinito reservoir (NW Mexico) before and after dam construction using physical sediment analyses, Journal of South American Earth Sciences, 111, doi:10.1016/j.jsames.2021.103401.

Namier, N., et al. (2021), Mineral magnetic properties of loess-paleosol couplets of northern Serbia over the last 1.0 Ma, Quaternary Research, 103, 35-48, doi:10.1017/qua.2021.41.

Neelavannan, K., C. L. Narasimhan, K. Sivaraj, V. Nisha, and S. Sekar (2021), Environmental magnetic and textural characteristics of two estuarine core sediments from Bay of Bengal, India, Arabian Journal of Geosciences, 14(18), doi:10.1007/s12517-021-07785-x.

Ning, W. X., J. B. Zan, S. L. Yang, X. M. Fang, M. M. Shen, J. Kang, Y. L. Luo, and S. W. Wang (2021), A Combined Rock Magnetic and Meteorological Investigation of the Precipitation Boundary Across the Tibetan Plateau, Geophysical Research Letters, 48(18), doi:10.1029/2021gl094808.

Peng, J., X. Bai, and X. Chen (2021), Climate-driven soil erosion processes in alpine environments over the last century: Evidence from the Taibai Mountain (central China), Catena, 206, doi:10.1016/j.catena.2021.105569.

Qian, Y., D. Heslop, A. P. Roberts, P. X. Hu, X. Zhao, Y. Liu, J. H. Li, K. M. Grant, and E. J. Rohling (2021), Low-Temperature Magnetic Properties of Marine Sediments-Quantifying Magnetofossils, Superparamagnetism, and Maghemitization: Eastern Mediterranean Examples, Journal of Geophysical Research-Solid Earth, 126(9), doi:10.1029/2021jb021793.

Ustra, A. T., D. Ntarlagiannis, L. Sagnotti, and L. Jovane (2021), Editorial: Bridging Environmental Magnetism With Biogeophysics to Study Biogeochemical Processes of Today, Frontiers in Earth Science, 9, doi:10.3389/feart.2021.757171.

Wang, Z. X., C. J. Huang, D. B. Kemp, Z. Zhang, and Y. Sui (2021), Distinct responses of late Miocene eolian and lacustrine systems to astronomical forcing in NE Tibet, Geological Society of America Bulletin, 133(11-12), 2266-2278, doi:10.1130/b35776.1.

Wu, C., H. Long, T. Cheng, L. Liu, P. Qian, H. Wang, S. F. Ren, L. M. Zhou, and X. M. Zheng (2021a), Quantitative estimations of iron oxide minerals in the Late Pleistocene paleosol of the Yangtze River Delta: Implications for the chemical weathering, sedimentary environment, and burial conditions, Catena, 207, doi:10.1016/j.catena.2021.105662.

Wu, D., C. B. Zhang, T. Wang, L. Liu, X. J. Zhang, Z. J. Yuan, S. L. Yang, and F. H. Chen (2021b), East-west asymmetry in the distribution of rainfall in the Chinese Loess Plateau during the Holocene, Catena, 207, doi:10.1016/j.catena.2021.105626.

Yang, H., G. Q. Li, S. Y. Gou, J. K. Qian, Y. Q. Deng, Y. N. Zhang, T. N. Jonell, Z. Wang, and M. Jin (2021), The close-space luminescence dated loess record from SW Junggar Basin indicates persistent aridity during the last glacial-interglacial cycle in lowlands of Central Asia, Palaeogeography Palaeoclimatology Palaeoecology, 584, doi:10.1016/j.palaeo.2021.110664.

Yang, S. L., X. J. Liu, T. Cheng, Y. L. Luo, Q. Li, L. Liu, and Z. X. Chen (2021), Stepwise Weakening of Aeolian Activities During the Holocene in the Gannan Region, Eastern Tibetan Plateau, Frontiers in Earth Science, 9, doi:10.3389/feart.2021.686677.

Zhang, Q., E. Appel, N. Basavaiah, S. Y. Hu, X. H. Zhu, and U. Neumann (2021b), Is Alteration of Magnetite During Rock Weathering Climate-Dependent?, Journal of Geophysical Research-Solid Earth, 126(10), doi:10.1029/2021jb022693.

Zhang, Q., Q. S. Liu, A. P. Roberts, J. M. Yu, Y. Liu, and J. H. Li (2021b), Magnetotactic Bacterial Activity in the North Pacific Ocean and Its Relationship to Asian Dust Inputs and Primary Productivity Since 8.0 Ma, Geophysical Research Letters, 48(15), doi:10.1029/2021gl094687.

Zhou, D. Y., G. H. Shi, S. Z. Liu, and B. L. Wu (2021), Mineralogy and Magnetic Behavior of Yellow to Red Xuanhua-Type Agate and Its Indication to the Forming Condition, Minerals, 11(8), doi:10.3390/min11080877.

Extraterrestrial and Planetary Magnetism

Hewins, R. H., et al. (2021a), Northwest Africa (NWA) 12563 and ungrouped C2 chondrites: Alteration styles and relationships to asteroids, Geochimica Et Cosmochimica Acta, 311, 238-273, doi:10.1016/j.gca.2021.06.035.

Hewins, R. H., et al. (2021b), Magnetite-rich c2-ung chondrites and their asteroidal parent bodies, Meteoritics & Planetary Science, 56.

O'Neill, C. (2021), End-Member Venusian Core Scenarios: Does Venus Have an Inner Core?, Geophysical Research Letters, 48(17), doi:10.1029/2021gl095499.

Sridhar, S., J. F. J. Bryson, A. J. King, and R. J. Harrison (2021), Constraints on the ice composition of carbonaceous chondrites from their magnetic mineralogy, Earth and Planetary Science Letters, 576, doi:10.1016/j.epsl.2021.117243.

Weisberg, M. K., M. E. Zolensky, M. Kimura, K. T. Howard, D. S. Ebel, M. L. Gray, and C. Alexander (2021), Magnetite in matrix of anomalous el3 chondrite Northwest Africa (NWA) 8785, Meteoritics & Planetary Science, 56.

Fundamental Rock Magnetism and direct Applications

Badejo, S. A., A. J. Fraser, M. Neumaier, A. R. Muxworthy, and J. R. Perkins (2021a), 3D petroleum systems modelling as an exploration tool in mature basins: A study from the Central North SeaUK, Marine and Petroleum Geology, 133, doi:10.1016/j.marpetgeo.2021.105271.

Badejo, S. A., A. R. Muxworthy, A. Fraser, M. Neumaier, J. R. Perkins, G. R. Stevenson, and R. Davey (2021b), Using magnetic techniques to calibrate hydrocarbon migration in petroleum systems modelling: a case study from the Lower Tertiary, UK Central North Sea, Geophysical Journal International, 227(1), 617-631, doi:10.1093/gji/ggab236.

Dunlop, D. J. (2021), Magnetic hysteresis of magnetite at high temperature: grain size variation, Geophysical Journal International, 226(2), 816-827, doi:10.1093/gji/ggab138.

Jeong, J. O., H. S. Ahn, M. Son, H. Cho, and Y. K. Sohn (2021), Eruptive and depositional processes of a low-aspect-ratio ignimbrite (the Southern Kusandong Tuff, South Korea) inferred from magnetic susceptibility variability, Journal of Volcanology and Geothermal Research, 419, doi:10.1016/j.jvolgeores.2021.107374.

Petronis, M. S., M. Awdankiewicz, J. Valenta, V. Rapprich, J. P. Zebrowski, and E. Karim (2021), Eruptive and magma feeding system evolution of Sosnica Hill Volcano (Lower Silesia, SW Poland) revealed from Volcanological, Geophysical, and Rock Magnetic Data, Journal of Volcanology and Geothermal Research, 419, doi:10.1016/j.jvolgeores.2021.107367.

Robinson, P., S. A. McEnroe, R. J. Harrison, K. Fabian, F. Heidelbach, and M. Jackson (2021), Lamellar magnetism and exchange bias in billion-year-old metamorphic titanohematite with nanoscale ilmenite exsolution lamellae - III Atomic-magnetic basis for experimental results, Geophysical Journal International, 226(2), 1348-1367, doi:10.1093/gji/ggab176.

Sprain, C. J., J. M. Feinberg, R. Lamers, and R. K. Bono (2021), Characterization of Magnetic Mineral Assemblages in Clinkers: Potential Tools for Full Vector Paleomagnetic Studies, Geochemistry Geophysics Geosystems, 22(9), doi:10.1029/2021gc009795.

Zu, Q., C. H. Chen, C. R. Chen, S. Liu, and H. Y. Yen (2021), The relationship among earthquake location, magnetization, and subsurface temperature beneath the Taiwan areas, Physics of the Earth and Planetary Interiors, 320, doi:10.1016/j.pepi.2021.106800.

Geomagnetism, Paleointensity and Records of the Geomagnetic Field

Arneitz, P., R. Leonhardt, R. Egli, and K. Fabian (2021), Dipole and Nondipole Evolution of the Historical Geomagnetic Field From Instrumental, Archeomagnetic, and Volcanic Data, Journal of Geophysical Research-Solid Earth, 126(10), doi:10.1029/2021jb022565.

Bonilla-Alba, R., et al. (2021), Rapid Intensity Decrease During the Second Half of the First Millennium BCE in Central Asia and Global Implications, Journal of Geophysical Research-Solid Earth, 126(10), doi:10.1029/2021jb022011.

Cych, B., M. Morzfeld, and L. Tauxe (2021), Bias Corrected Estimation of Paleointensity (BiCEP): An Improved Methodology for Obtaining Paleointensity Estimates, Geochemistry Geophysics Geosystems, 22(8), doi:10.1029/2021gc009755.

Davies, C. J., R. K. Bono, D. G. Meduri, J. Aubert, S. Greenwood, and A. J. Biggin (2022), Dynamo constraints on the long-term evolution of Earth's magnetic field strength, Geophysical Journal International, 228(1), 316-336, doi:10.1093/gji/ggab342.

Di Mauro, D., M. Regi, S. Lepidi, A. Del Corpo, G. Dominici, P. Bagiacchi, G. Benedetti, and L. Cafarella (2021), Geomagnetic Activity at Lampedusa Island: Characterization and Comparison with the Other Italian Observatories, Also in Response to Space Weather Events, Remote Sensing, 13(16), doi:10.3390/rs13163111.

Garcia-Redondo, N., M. Calvo-Rathert, A. Carrancho, A. Goguitchaichvili, E. Iriarte, A. Blanco-Gonzalez, M. J. Dekkers, J. Morales-Contreras, C. Alario-Garcia, and C. Macarro-Alcalde (2021), Further Evidence of High Intensity During the Levantine Iron Age Anomaly in Southwestern Europe: Full Vector Archeomagnetic Dating of an Early Iron Age Dwelling From Western Spain, Journal of Geophysical Research-Solid Earth, 126(9), doi:10.1029/2021jb022614.

Inoue, K., T. Yamazaki, and Y. Usui (2021), Influence of Magnetofossils on Paleointensity Estimations Inferred From Principal Component Analyses of First-Order Reversal Curve Diagrams for Sediments From the Western Equatorial Pacific, Geochemistry Geophysics Geosystems, 22(10), doi:10.1029/2021gc010081.

Kapawar, M. R., and V. Mamilla (2021), Paleointensity of the Earth's magnetic Beld at similar to 117 Ma determined from the Rajmahal and Sylhet Trap Basalts, India, Journal of Earth System Science, 130(3), doi:10.1007/s12040-021-01652-9.

Kirscher, U., E. Dallanave, V. Weissbrodt, P. Stojakowits, M. Grau, V. Bachtadse, and C. Mayr (2021), The Laschamps geomagnetic excursion recorded in continental sediments from southern Germany, Geophysical Journal International, 227(2), 1354-1365, doi:10.1093/gji/ggab276.

Larocca, P., M. A. Arecco, and M. Mora (2021), wavelet-based characterization of seismicity and geomagnetic disturbances in the South Sandwich microplate area, Geofisica Internacional, 60(4), 320-332, doi:10.22201/igeof.00167169p.2021.60.4.2119.

Levashova, N. M., I. V. Golovanova, D. V. Rud'ko, K. N. Danukalov, S. V. Rud'ko, R. Y. Sal'manova, and N. D. Sergeeva (2021), Late Ediacaran Hyperactivity Period: Quantifying the Reversal Frequency, Izvestiya-Physics of the Solid Earth, 57(2), 247-256, doi:10.1134/s1069351321020026.

Lloyd, S. J., A. J. Biggin, and Z. X. Li (2021), New Paleointensity Data Suggest Possible Phanerozoic-Type Paleomagnetic Variations in the Precambrian, Geochemistry Geophysics Geosystems, 22(10), doi:10.1029/2021gc009990.

Lund, S. P. (2020), Regional character of geomagnetic field directional circularity: Holocene East Asia, Physics of the Earth and Planetary Interiors, 308, doi:10.1016/j.pepi.2020.106572.

Lund, S., G. Acton, B. Clement, M. Okada, and L. Keigwin (2021), On the relationship between paleomagnetic secular variation and excursions-Records from MIS 6 and 7-ODP Leg 172, Physics of the Earth and Planetary Interiors, 318, doi:10.1016/j.pepi.2021.106727.

Oliveira, W. P., et al. (2021), Paleosecular Variation and the Time-Averaged Geomagnetic Field Since 10 Ma, Geochemistry Geophysics Geosystems, 22(10), doi:10.1029/2021gc010063.

Schnepp, E., P. Arneitz, M. Ganerod, R. Scholger, I. Fritz, R. Egli, and R. Leonhardt (2021), Intermediate field directions recorded in Pliocene basalts in Styria (Austria): evidence for cryptochron C2r.2r-1, Earth Planets and Space, 73(1), doi:10.1186/s40623-021-01518-w.

Thallner, D., A. J. Biggin, P. J. A. McCausland, and R. R. Fu (2021), New Paleointensities From the Skinner Cove Formation, Newfoundland, Suggest a Changing State of the Geomagnetic Field at the Ediacaran-Cambrian Transition, Journal of Geophysical Research-Solid Earth, 126(9), doi:10.1029/2021jb022292.

Wang, W. Z., T. von Dobeneck, T. Frederichs, Y. Zhang, L. Lembke-Jene, R. Tiedemann, M. Winklhofer, and D. Nurnberg (2021), Dating North Pacific Abyssal Sediments by Geomagnetic Paleointensity: Implications of Magnetization Carriers, Plio-Pleistocene Climate Change, and Benthic Redox Conditions, Frontiers in Earth Science, 9, doi:10.3389/feart.2021.683177.

Wang, W. Z., T. von Dobeneck, T. Frederichs, Y. Zhang, L. Lembke-Jene, R. Tiedemann, M. Winklhofer, and D. Nurnberg (2021), Dating North Pacific Abyssal Sediments by Geomagnetic Paleointensity: Implications of Magnetization Carriers, Plio-Pleistocene Climate Change, and Benthic Redox Conditions, Frontiers in Earth Science, 9, doi:10.3389/feart.2021.683177.

Zhang, R., et al. (2021c), "Tiny Wiggles" in the Late Miocene Red Clay Deposits in the North-East of the Tibetan Plateau, Geophysical Research Letters, 48(16), doi:10.1029/2021gl093962.

Magnetic Fabrics and Anisotropy

Agarwal, A., D. C. Srivastava, J. Shah, and M. A. Mamtani (2021), Magnetic fabrics in an apparently undeformed granite body near Main Boundary Thrust (MBT), Kumaun Lesser Himalaya, India, Tectonophysics, 815, doi:10.1016/j.tecto.2021.228996.

Ananth, C., and S. Bhadra (2021), Origin and tectonic implications of a new Belur-Sarkar Nattar Mangalam-Udayapatti shear zone (BNUSZ), Salem Granulite Block, India: Insights from deformation and magnetic fabrics, Journal of Earth System Science, 130(4), doi:10.1007/s12040-021-01717-9.

Archanjo, C. J., C. A. Salazar, F. P. Caltabellota, and S. W. O. Rodrigues (2021), The onset of the right-lateral strike-slip setting recorded in magnetic fabrics of A-type granite plutons of the Ribeira belt (SE Brazil), Precambrian Research, 366, doi:10.1016/j.precamres.2021.106417.

Biedermann, A. R., M. Pugnetti, and Y. Zhou (2021), Explaining the large variability in empirical relationships between magnetic pore fabrics and pore space properties, Geophysical Journal International, 227(1), 496-517, doi:10.1093/gji/ggab230.

Burgin, H. B., P. Robion, and K. Amrouch (2021), Layer parallel stretching? Characterising magnetic and pore-fabric styles at a rifted continental margin: New insights from the Otway Ranges, Australia, Tectonophysics, 815, doi:10.1016/j.tecto.2021.228975.

Das, A., J. Mallik, and S. Banerjee (2021), Characterization of the magma flow direction in the Nandurbar-Dhule Deccan dyke swarm inferred from magnetic fabric analysis, Physics of the Earth and Planetary Interiors, 319, doi:10.1016/j.pepi.2021.106782.

Garcia-Amador, B. I., L. M. Alva-Valdivia, and A. Hernandez-Cardona (2021), Syn-tectonic Dipilto batholith (NW Nicaragua) linked to arc-continent collision: High- and room-temperature AMS evidence, Tectonophysics, 815, doi:10.1016/j.tecto.2021.229000.

Kleuser, E., C. E. D. Barros, C. J. Archanjo, B. C. Dressel, and L. G. de Castro (2021), Anisotropy of magnetic susceptibility, gravimetry and geochronology of the Cerne granite, Ribeira Belt, southern Brazil, Journal of South American Earth Sciences, 112, doi:10.1016/j.jsames.2021.103536.

Oliva-Urcia, B., J. Lopez-Martinez, A. Maestro, A. Gil, T. Schmid, L. J. Lamban, C. Gale, T. Ubide, and M. Lago (2021), Magnetic fabric from Quaternary volcanic edifices in the extensional Bransfield Basin: internal structure of Penguin and Bridgeman islands (South Shetlands archipelago, Antarctica), Geophysical Journal International, 226(2), 1368-1389, doi:10.1093/gji/ggab177.

Saur, H., P. Moonen, and C. Aubourg (2021), Grain Fabric Heterogeneity in Strained Shales: Insights From XCT Measurements, Journal of Geophysical Research-Solid Earth, 126(9), doi:10.1029/2021jb022025.

Other

Chen, S. A., P. J. Heaney, J. E. Post, T. B. Fischer, P. J. Eng, and J. E. Stubbs (2021), Superhydrous hematite and goethite: A potential water reservoir in the red dust of Mars?, Geology, 49(11), 1343-1347, doi:10.1130/g48929.1.

Groot, L. V., K. Fabian, A. Beguin, M. E. Kosters, D. Cortes-Ortuno, R. R. Fu, C. M. L. Jansen, R. J. Harrison, T. Leeuwen, and A. Barnhoorn (2021), Micromagnetic Tomography for Paleomagnetism and Rock-Magnetism, Journal of Geophysical Research-Solid Earth, 126(10), doi:10.1029/2021jb022364.

Jones, S. A., E. Blinman, L. Tauxe, J. R. Cox, S. Lengyel, R. Sternberg, J. Eighmy, D. Wolfman, and R. DuBois (2021), MagIC as a FAIR Repository for America's Directional Archaeomagnetic Legacy Data, Journal of Geophysical Research-Solid Earth, 126(10), doi:10.1029/2021jb022874.

Krot, A. N., M. I. Petaev, and K. Nagashima (2021), Infiltration metasomatism of the Allende coarse-grained calcium-aluminum-rich inclusions, Progress in Earth and Planetary Science, 8(1), doi:10.1186/s40645-021-00437-4.

Paleomagnetism

Biasi, J., and L. Karlstrom (2021), Timescales of magma transport in the Columbia River flood basalts, determined by paleomagnetic data, Earth and Planetary Science Letters, 576, doi:10.1016/j.epsl.2021.117169.

Boschman, L. M., D. J. J. Van Hinsbergen, C. G. Langereis, K. E. Flores, P. J. J. Kamp, D. L. Kimbrough, H. Ueda, S. H. A. Van de Lagemaat, E. Van der Wiel, and W. Spakman (2021), Reconstructing lost plates of the Panthalassa ocean through paleomagnetic data from circum-pacific accretionary orogens, American Journal of Science, 321(6), 907-954, doi:10.2475/06.2021.08.

Dembo, N., Y. Hamiel, and R. Granot (2021), The stepovers of the Central Dead Sea Fault: What can we learn from the confining vertical axis rotations?, Tectonophysics, 816, doi:10.1016/j.tecto.2021.229036.

Gong, Z., et al. (2021), Reorienting the West African craton in Paleoproterozoic- Mesoproterozoic supercontinent Nuna, Geology, 49(10), 1171-1176, doi:10.1130/g48855.1.

Li, B. S., M. D. Yan, W. L. Zhang, and X. M. Fang (2021), Bidirectional growth of the Altyn Tagh Fault since the Early Oligocene, Tectonophysics, 815, doi:10.1016/j.tecto.2021.228991.

Liu, W., et al. (2021), Coeval Evolution of the Eastern Philippine Sea Plate and the South China Sea in the Early Miocene: Paleomagnetic and Provenance Constraints From ODP Site 1177, Geophysical Research Letters, 48(14), doi:10.1029/2021gl093916.

Makaroglu, O. (2021), A Holocene paleomagnetic record from Kucukcekmece Lagoon, NW Turkey, Turkish Journal of Earth Sciences, 30(5), 639-652, doi:10.3906/yer-2102-13.

Martins, P. L. G., C. L. B. Toledo, A. M. Silva, P. Y. J. Antonio, F. Chemale, L. M. Assis, and R. I. F. Trindade (2021), Low paleolatitude of the Carajas Basin at similar to 2.75 Ga: Paleomagnetic evidence from basaltic flows in Amazonia, Precambrian Research, 365, doi:10.1016/j.precamres.2021.106411.

Morley, C. K., S. Chantraprasert, J. Kongchum, and K. Chenoll (2021), The West Burma Terrane, a review of recent paleo-latitude data, its geological implications and constraints, Earth-Science Reviews, 220, doi:10.1016/j.earscirev.2021.103722.

Rapalini, A. E., F. Poblete, C. C. Miranda, and M. I. B. Raposo (2021), New advances in paleomagnetic and magnetic fabric studies in Latin America: An introduction, Journal of South American Earth Sciences, 111, doi:10.1016/j.jsames.2021.103431.

Ren, Q., S. H. Zhang, T. Sukhbaatar, H. Q. Zhao, H. C. Wu, T. S. Yang, H. Y. Li, Y. J. Gao, and X. C. Jin (2021), Did the Boreal Realm extend into the equatorial region? New paleomagnetic evidence from the Tuva-Mongol and Amuria blocks, Earth and Planetary Science Letters, 576, doi:10.1016/j.epsl.2021.117246.

Robert, B., M. Domeier, and J. Jakob (2021), On the origins of the Iapetus ocean, Earth-Science Reviews, 221, doi:10.1016/j.earscirev.2021.103791.

Salminen, J., S. A. Elming, S. Mertanen, C. Wang, B. Almqvist, and M. O. Moakhar (2021), Paleomagnetic studies of rapakivi complexes in the Fennoscandian shield Implications to the origin of Proterozoic massif-type anorthosite magmatism, Precambrian Research, 365, doi:10.1016/j.precamres.2021.106406.

Wabo, H., N. J. Beukes, S. Patranabis-Deb, D. Saha, G. Belyanin, and J. Kramers (2022), Paleomagnetic and Ar-40/Ar-39 age constraints on the timing of deposition of deep-water carbonates of the Kurnool Group (Cuddapah basin) and correlation across Proterozoic Purana successions of Southern India, Journal of Asian Earth Sciences, 223, doi:10.1016/j.jseaes.2021.104984.

Wils, K., M. Deprez, C. Kissel, M. Vervoort, M. Van Daele, M. R. Daryono, V. Cnudde, D. H. Natawidjaja, and M. De Batist (2021), Earthquake doublet revealed by multiple pulses in lacustrine seismo-turbidites, Geology, 49(11), 1301-1306, doi:10.1130/g48940.1.

Xu, S. H., X. X. Zhao, Y. X. Li, X. Y. Liu, and W. W. Chen (2021), Pulsed vertical displacement and subsequent shearing in the forearc of the Costa Rican convergent margin: Evidence from paleomagnetic results of IODP site U1413, Marine Geology, 441, doi:10.1016/j.margeo.2021.106606.

Xu, W., W. H. Ji, B. Song, Y. Li, Y. Zhao, B. W. Wang, H. Y. Zhang, X. Z. Ye, X. Y. Wei, and P. McLachlan (2021), Primary Carboniferous paleomagnetic and geochronologic results from the Aqishan-Yamansu Belt, Eastern Tianshan: Implications for the tectonic evolution of the Paleo-Asian Ocean, Tectonophysics, 818, doi:10.1016/j.tecto.2021.229070.

Zhang, D. H., B. C. Huang, G. C. Zhao, J. G. Meert, S. Williams, J. Zhao, and T. H. Zhou (2021a), Quantifying the Extent of the Paleo-Asian Ocean During the Late Carboniferous to Early Permian, Geophysical Research Letters, 48(15), doi:10.1029/2021gl094498.

Zhang, D. H., B. C. Huang, J. G. Meert, G. C. Zhao, J. Zhao, and Q. Zhao (2021a), Micro-Blocks in NE Asia Amalgamated Into the Unified Amuria Block by similar to 300 Ma: First Paleomagnetic Evidence From the Songliao Block, NE China, Journal of Geophysical Research-Solid Earth, 126(10), doi:10.1029/2021jb022881.

Zhao, P., J. Y. He, C. L. Deng, Y. Chen, and R. N. Mitchell (2021), Early Neoproterozoic (870-820 Ma) amalgamation of the Tarim craton (northwestern China) and the final assembly of Rodinia, Geology, 49(11), 1277-1282, doi:10.1130/g48837.1.

Stratigraphy

Artiaga, D., J. Garcia-Veigas, D. I. Cendon, C. Atalar, and L. Gibert (2021), The Messinian evaporites of the Mesaoria basin (North Cyprus): A discrepancy with the current chronostratigraphic understanding, Palaeogeography Palaeoclimatology Palaeoecology, 584, doi:10.1016/j.palaeo.2021.110681.

Crow, R. S., J. Schwing, K. E. Karlstrom, M. Heizler, P. A. Pearthree, P. K. House, S. Dulin, S. U. Janecke, M. Stelten, and L. J. Crossey (2021), Redefining the age of the lower Colorado River, southwestern United States, Geology, 49(9), E532-E533, doi:10.1130/g49334y.1.

Cullen, T. M., R. E. L. Collier, D. M. Hodgson, R. L. Gawthorpe, K. Kouli, M. Maffione, H. Kranis, and G. T. Eliassen (2021), Deep-Water Syn-rift Stratigraphy as Archives of Early-Mid Pleistocene Palaeoenvironmental Signals and Controls on Sediment Delivery, Frontiers in Earth Science, 9, doi:10.3389/feart.2021.715304.

Feng, Z. T., W. L. Zhang, X. M. Fang, J. B. Zan, T. Zhang, C. H. Song, and M. D. Yan (2022), Eocene deformation of the NE Tibetan Plateau: Indications from magnetostratigraphic constraints on the oldest sedimentary sequence in the Linxia Basin, Gondwana Research, 101, 77-93, doi:10.1016/j.gr.2021.07.027.

Guzhikov, A. Y., E. Y. Baraboshkin, G. N. Aleksandrova, I. P. Ryabov, M. A. Ustinova, L. F. Kopaevich, G. V. Mirantsev, A. B. Kuznetsov, P. A. Fokin, and V. L. Kosorukov (2021), Bio-, Chemo-, and Magnetostratigraphy of the Santonian-Campanian Boundary in the Kudrino and Aksu-Dere Sections (Southwestern Crimea): Problems of Global Correlation and Selection of the Lower Boundary Stratotype of the Campanian. 2. Magneto- and Chemostratigraphy, Discussion, Stratigraphy and Geological Correlation, 29(5), 518-547, doi:10.1134/s086959382105004x.

Haque, Z., J. W. Geissman, P. G. DeCelles, and B. Carrapa (2021), A magnetostratigraphic age constraint for the proximal synorogenic conglomerates of the Late Cretaceous Cordilleran foreland basin, northeast Utah, USA, Geological Society of America Bulletin, 133(9-10), 1795-1814, doi:10.1130/b35768.1.

Haque, Z., J. W. Geissman, R. B. Irmis, P. E. Olsen, C. Lepre, H. Buhedma, R. Mundil, W. G. Parker, C. Rasmussen, and G. E. Gehrels (2021), Magnetostratigraphy of the Triassic Moenkopi Formation From the Continuous Cores Recovered in Colorado Plateau Coring Project Phase 1 (CPCP-1), Petrified Forest National Park, Arizona, USA: Correlation of the Early to Middle Triassic Strata and Biota in Colorado Plateau and Its Environs, Journal of Geophysical Research-Solid Earth, 126(9), doi:10.1029/2021jb021899.

He, C. C., Y. Q. Zhang, S. K. Li, K. Wang, and J. Q. Ji (2021), Magnetostratigraphic study of a Late Cretaceous-Paleogene succession in the eastern Xining basin, NE Tibet: Con-

straint on the timing of major tectonic events in response to the India-Eurasia collision, Geological Society of America Bulletin, 133(11-12), 2457-2484, doi:10.1130/b35874.1.

Head, M. J. (2021), Review of the Early-Middle Pleistocene boundary and Marine Isotope Stage 19, Progress in Earth and Planetary Science, 8(1), doi:10.1186/s40645-021-00439-2.

Hofken, A. F., T. von Dobeneck, T. Kuhn, and S. Kasten (2021), Impact of Upward Oxygen Diffusion From the Oceanic Crust on the Magnetostratigraphy and Iron Biomineralization of East Pacific Ridge-Flank Sediments, Frontiers in Earth Science, 9, doi:10.3389/feart.2021.689931.

Lauchli, C., et al. (2021), Magnetostratigraphy and stable isotope stratigraphy of the middle-Eocene succession of the Ainsa basin (Spain): New age constraints and implications for sediment delivery to the deep waters, Marine and Petroleum Geology, 132, doi:10.1016/j.marpetgeo.2021.105182.

Llanos, M. P. I., and D. A. Kietzmann (2020), Magnetostratigraphy of the Jurassic Through Lower Cretaceous in the Neuquen Basin, in Opening and Closure of the Neuquen Basin in the Southern Andes, edited by D. Kietzmann and A. Folguera, pp. 175-210, doi:10.1007/978-3-030-29680-3_8.

Remin, Z., M. Cyglicki, M. Barski, Z. Dubicka, and J. Roszkowska-Remin (2021), The K-Pg boundary section at Nasilow, Poland: stratigraphic reassessment based on foraminifers, dinoflagellate cysts and palaeomagnetism, Geological Quarterly, 65(3), doi:10.7306/gq.1614.

Seiriene, V., A. Karabanov, V. Baltrunas, B. Karmaza, V. Katinas, V. Pukelyte, T. Rylova, and S. Demidova (2021), Correlation of Eemian sections in Lithuania and Belarus based on palaeomagnetic, radioisotope and palaeobotanic data, Geological Quarterly, 65(3), doi:10.7306/gq.1615.

Suganuma, Y., et al. (2021), Formal ratification of the Global Boundary Stratotype Sec- tion and Point (GSSP) for the Chibanian Stage and Middle Pleistocene Subseries of the Quaternary System: the Chiba Section, Japan dagger, Episodes, 44(3), 317-347, doi:10.18814/epiiugs/2020/020080.

Ucar, H., G. Kletetschka, and J. Kadlec (2021), Evidence of the Matuyama-Brunhes transition in cave sediment in Central Europe, Quaternary International, 604, 16-27, doi:10.1016/j.quaint.2021.07.005.

Relax!

Michael (Ted) Evans
University of Alberta, Canada
tedevans.evans403@gmail.com

In an earlier IRMQuarterly (24/3 Fall 2014), I mused about the potential for an IRMDaily—with a bumper edition for the weekend. I was driven to the idea by the manner in which the number of enviromagnetic papers was shooting up. The passage of time has indicated that this was a fine example of Mark Twain's dictum to the effect that astonishing returns can be had from trifling investment of facts. Figure 1 makes the point... hard on the heels of my analysis, the real story emerged.

After a growth spurt, the topic settled into maturity—and so far, there's no sign of old age (or even a mid-life crisis). What does this mature phase look like? Well, the paper-a-day scenario has not come to pass. In fact, we can take the weekend off, and plod along at a paper every two days.

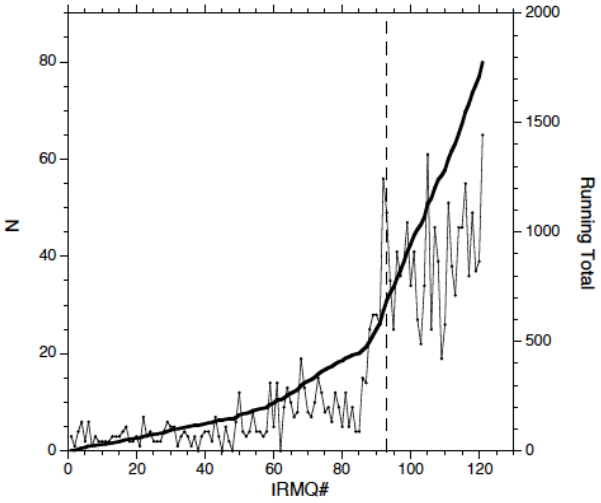

Figure 1: Number of enviromagnetic papers listed in IRM Quarterly from #1(Vol.1.1, Spring 1991) to #121(Vol.31.2, Summer 2021). The vertical dashed line indicates the date of my earlier note.

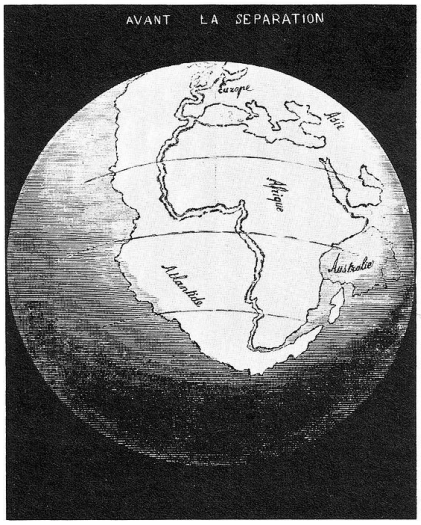

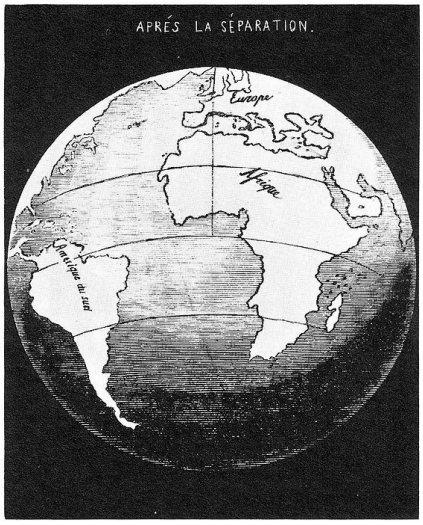

cont'd. from pg. 1...
ferromagnetic minerals such as hematite. If these minerals show a crystallographic-preferred orientation (CPO), they will contribute to the magnetic fabric of the rock (Biedermann, 2018; Finke, 1909; König, 1887; Stenger, 1888; Tyndall, 1851).

Shape anisotropy, as the name implies, is controlled by grain shape and related distribution of surface charges, which control the grain's self-demagnetizing field. Therefore, the easy magnetization direction is along the longest axis of the grain (Osborn, 1945; Stoner, 1945). Shape anisotropy occurs in non-isometric grains with strong magnetization and is the dominant source of anisotropy in magnetite. Magnetite grains with a shape-preferred orientation (SPO) contribute to magnetic fabrics in rocks.

Distribution anisotropy results from magnetostatic interactions of strongly magnetic minerals with a non-uniform distribution within a rock, e.g., a preferential concentration along specific planes arising from compositional banding. The crystals themselves may or may not be particularly anisotropic or preferentially aligned, but their interactions give rise to strong anisotropy along the specific planes/distributions (Cañón-Tapia, 1996, 2001; Hargraves et al., 1991; Rochette et al., 1999).

It is important to note that strongly anisotropic minerals (e.g., uniaxial magnetite crystals) that are randomly oriented and spatially uniformly distributed in a rock will give rise to an isotropic fabric, whereas weakly anisotropic, but strongly aligned (e.g., olivine) or non-uniformly distributed minerals (e.g., equant magnetite grains), will result in strongly anisotropic fabrics (Figure 1). Therefore, in addition to the specific crystal properties or grain shape that set an upper limit to the bulk anisotropy, mineral alignment and distribution are also important, resulting in a gamut of possibilities when interpreting magnetic fabrics.

Too often these possibilities are overlooked or oversimplified, leading to the potentially equivocal interpretations that this article aims at demystifying, so without much ado we will proceed to describe the different magnetic techniques available to characterize the anisotropies of specific mineral classes, the relation between bulk measurements and the anisotropy carriers, and how to best-interpret data within confidence.

Minerals/grain populations targeted by different anisotropy methods

Low-Field AMS (LF-AMS) is calculated based on the angular dependence of the initial susceptibility, acquired over typical fields of ~200-300 A/m, and frequencies of ~1 kHz. At these very low fields, all the minerals present in a sample are activated but far from saturated, so that their remanent magnetizations are not affected and the method is entirely non-destructive. LF-AMS is thus a superposition of various components, which does not allow separating the different contributions to the fabric.

Therefore, what minerals dominate LF-AMS? There is no one single answer to this question, not even when considering individual rock-types. The carriers of LF-AMS depend on the minerals present, their preferred orientation and spatial distribution. It is often assumed that magnetite tends to dominate LF-AMS: however, while magnetite present in small amounts does tend to dominate the sample's bulk properties, its contribution to the anisotropy is less straightforward. For example, if magnetite is isometric and (spatially) randomly distributed, it will not contribute to anisotropy. Magnetite anisotropy is also grain-size dependent: Stable single domain (SSD) magnetite grains, which are very important in paleomagnetism, are magnetically saturated by definition and therefore carry no susceptibility parallel to their easy axes, resulting in low bulk susceptibility and inverse magnetic fabrics if preferentially aligned (e.g., Potter & Stephenson, 1988). On the contrary, multidomain (MD) magnetite grains, while generally avoided for paleomagnetic studies, tend to have higher susceptibility and contribute substantially to LF-AMS if non-randomly aligned and/or distributed. The paramagnetic and diamagnetic mineral fractions also contribute to, and may even dominate, the LF-AMS, depending on their single crystal properties and alignment. Likewise, while not carrying particularly important low-field susceptibility, aligned particles of weakly ferromagnetic hematite may be an important carrier of LF-AMS in virtue of their strong magnetocrystalline anisotropy. Note, however, that particle magnetostatic interactions are considered to be negligible for hematite.

Low-temperature (LT) LF-AMS is sometimes used to enhance the paramagnetic contribution to LF-AMS (Issachar et al., 2016, 2018; Parés & van der Pluijm, 2002). While diamagnetic susceptibility and its anisotropy is largely temperature-independent, paramagnetic susceptibility has an inverse relationship with temperature, following the Curie-Weiss law $M = C\,(B/T)$. Likewise, many natural ferromagnetic minerals undergo mineralogical transitions between RT and LT (77 K) measurements. Below the Morin transition, T_M, ~260 K, hematite's easy axis of magnetization rotates from within the basal plane to perpendicular to it, with sublattice spins becoming perfectly antiparallel and the only (weak) remanence arising from defects in the crystal structure (e.g., Bowles et al., 2010). Magnetite crystals undergo a structural change at the Verwey transition, T_V, where the crystal symmetry changes from cubic ($T > T_V$) to monoclinic ($T < T_V$), resulting in a loss of remanent magnetization when cooling through T_V (e.g., Jackson et al., 2011) and a drop in χ below T_V.

Therefore, LT-LF-AMS enhances the contribution of the paramagnetic phases while limiting that of the ferromagnets, though without entirely eliminating it. It is noteworthy that the contribution of SP grains, if present and depending on their blocking temperature, is enhanced at LT. Moreover, separation of the diamagnetic and paramagnetic contributions using LT-LF-AMS, while it has been proposed (Elhanati et al., 2021), is not

straightforward and results are not entirely unequivocal.

High Field AMS (HF-AMS) is calculated from stronger magnetizing fields, typically past the saturation of magnetite, in order to capture the paramagnetic high field *M*/*B* slope or susceptibility. The technique is typically employed for magnetite-bearing rocks since harder magnetic minerals such as hematite may not saturate in commonly available magnetic fields (typically in a torque-meter or vibrating sample magnetometer, VSM), in the range of ~1T and therefore complicate fabric separation.

Because paramagnetic moment increases linearly with field amplitude at commonly available laboratory high fields, HF-AMS is used to separate para/diamagnetic and ferromagnetic contributions. If HF-AMS is measured at both RT and LT, paramagnetic and diamagnetic components can be separated as well, however, this separation is limited by the comparable magnitudes of diamagnetic susceptibility and instrumental noise (Schmidt et al., 2007). Additionally, paramagnetic and ferromagnetic fabrics can be separated by LT-HF-AMS, e.g., using a torque-meter at liquid nitrogen temperatures, which is especially useful when the paramagnetic contribution is small at RT.

The fabric components isolated with the techniques detailed above will describe the anisotropy of all paramagnetic, all diamagnetic, and all ferromagnetic minerals, depending on which phases from each of the three magnetic classes are present. The contributions of the three classes can be separated from one another with reasonable confidence, however, complete removal of the ferromagnetic contribution may be difficult to ascertain when using HFs and/or LTs, especially when hematite or SP grains are present. Furthermore, it is important to note that even within each magnetic class, these contributions may again be superpositions. For example, the fabrics of amphibole and pyroxene, both paramagnetic, will both be captured by the same technique and be indistinguishable. Likewise, the ferromagnetic component characterized by HF-AMS captures all ferromagnetic minerals, including those that are not typically important remanence carriers, e.g., MD grains.

Remanence anisotropy can be measured by several methods that are based on the different kinds of laboratory magnetic remanences. All methods aim at characterizing the anisotropy of the remanence-carrying ferromagnetic minerals in the grain size/coercivity/blocking temperature range of interest and are therefore the most useful to isolate the specific anisotropy that is relevant to correct paleodirections and -intensities. Anisotropy of thermal remanence (ATRM) and anisotropy of anhysteretic remanence (AARM) magnetizations both use low DC fields that are comparable to the Earth's field (~0.05 mT) in conjunction with a randomizing force (temperature or alternating field, AF) to impart a remanence in a given temperature or coercivity window. Anisotropy of isothermal remanent magnetization (AIRM) uses variable pulsed or DC fields (mT to T) to impart stronger, typically saturating remanences. Thermal methods can

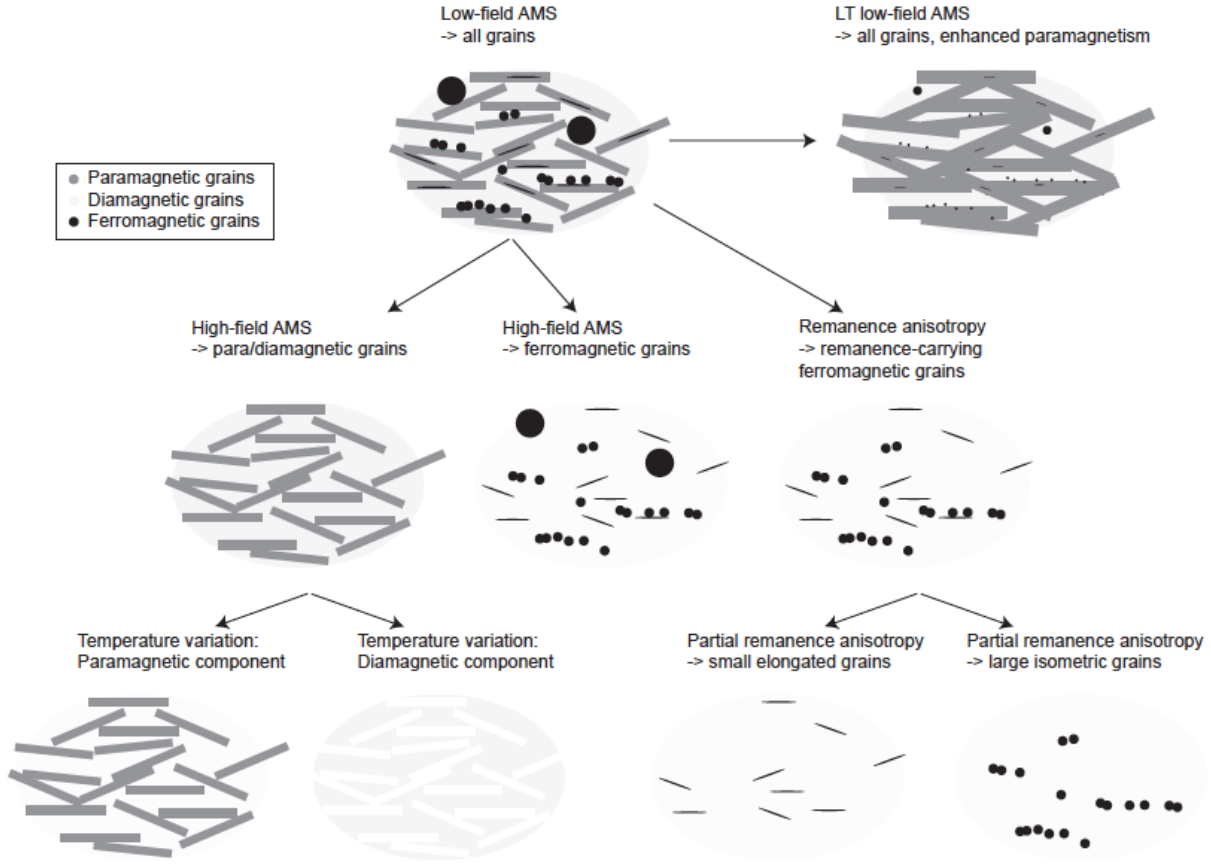

Figure 2: Schematic of magnetic mineral types targeted by different anisotropy measurements.

characterize the magnetic fabric of all remanence carriers but are prone to sample thermochemical alteration due to the repeated exposure to elevated temperatures. Anhysteretic remanence methods are mainly successful for low-coercivity minerals, where it is possible to target several sub-populations of grains using "low" AF field windows (≤ 200 mT), while higher-coercivity grains cannot be characterized due to most current instrument limitations. Isothermal methods can be used to determine magnetic fabrics of high-coercivity components, but because magnetization is not linear with field for the high fields used, approximations have to be made when processing the data with linear anisotropy theory.

Comparison between LF-AMS, HF-AMS and remanence anisotropy: Because the different magnetic anisotropy measurements target different mineral groups within a rock, a combination of methods can be used to better understand each group's contribution to the overall fabric (Figure 2). However, one needs to take particular care of the specific minerals and grain size populations that may be present, which will be preferentially targeted by the different techniques. For example, it is often reported that fabric coaxiality between LF-AMS and remanence anisotropy (e.g., AARM) is indicative of the same magnetite grains carrying the LF-AMS, however, this assumption is not always strictly valid and one must exercise caution.

Remanence anisotropy primarily targets SSD magnetite, which, owing to its higher M_{RS}/M_S ratio will particularly dominate the remanence over a range of applied field intensities/ targeted coercivities if both MD and SSD grains are present. On the other hand, LF-AMS is more sensitive to MD magnetite than SSD grains, and also includes the paramagnetic contribution to the anisotropy. Therefore, excluding the complications arising from inverse fabrics for preferentially aligned SSD grains, coaxiality between LF-AMS and AARM may either indicate that both fabrics are indeed carried by the same mineral in the same grain size distribution (e.g., only MD magnetite are present), or that different mineral grain sizes (fine and MD magnetite) are responsible for the same fabrics, or that the magnetite, in whichever of the two cases above, and paramagnetic fabrics have the same orientations. Conversely, the different orientation of LF-AMS and AARM may indicate that the paramagnetic and ferromagnetic minerals carry different fabrics, or it could reflect fine/SSD and MD magnetite populations with distinct anisotropies.

The two fabrics measured, whether co-axial or not, can therefore have very distinct origins. For these and other reasons it is particularly important to fully investigate the origin of magnetic fabrics.

Bulk susceptibility vs anisotropy carriers

When measuring LF-AMS, interpretations on its origin are often based on bulk magnetic properties such as mean susceptibility (K_{mean}), hysteresis or high- and low-temperature susceptibility curves. These, however, may not directly correlate with the AMS carrier minerals. Figure 3 from Pares (2015), for example, provides a useful "rule-of-thumb" tool to evaluate the contribution of different magnetic minerals to the bulk susceptibility in silicate-bearing rocks, clearly showing that even small concentrations of magnetite, for example, tend to dominate the bulk properties.

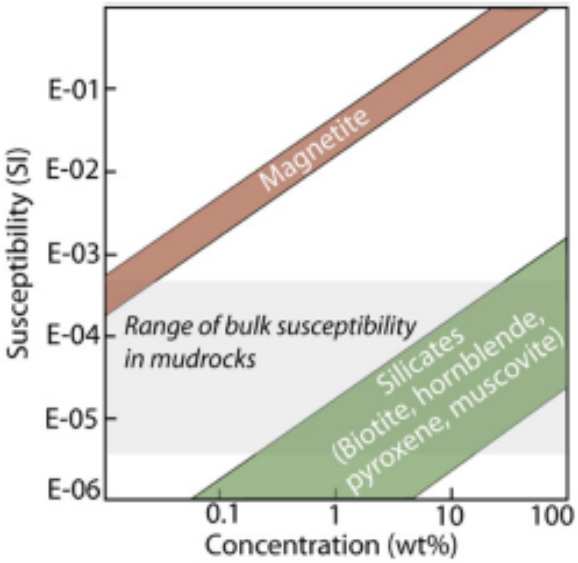

Figure 3: Simplified relationship between bulk susceptibility and concentration of different minerals contributing to the mean susceptibility (from Pares, 2015).

However, the fact that magnetite dominates K_{mean} does not always inform about the anisotropy carriers. Figures 1 and 4 show examples of rocks whose bulk properties are dominated by magnetite, but only in some of these does magnetite contribute to the anisotropy. Specifically, magnetite that does not have an SPO (randomly oriented grains) will not contribute to the anisotropy (Figure 1, top and Figure 4, left-hand side), yet the presence of magnetite, particularly MD, will result in high K_{mean} values, potentially leading to misinterpretation. In this case, the origin of LF-AMS must lie in another mineralogy and/or grain size, and we caution against making such assumptions.

Even without experimental fabric separation, it is possible in some cases to conclude that magnetite contributes to or dominates LF-AMS. The anisotropy displayed by minerals with magnetocrystalline anisotropy cannot be larger than that of the respective single crystals. Thus, if none of the other "matrix" minerals present possess large enough combined values of K_{mean} and degree of anisotropy, P, then it is likely that magnetite contributes to the anisotropy. Neither P nor K_{mean} alone, however, will be sufficient to unequivocally interpret the AMS-carriers. Further, a more adequate parameter to use is the mean deviatoric susceptibility, K', which directly indicates the contribution of a given mineral to the rock's anisotropy (Jelinek, 1984):

$$K' = \sqrt{\frac{(K_1 - K_{mean})^2 + (K_2 - K_{mean})^2 + (K_3 - K_{mean})^2}{3}}$$

Choice of parameters and data visualization will be cov-

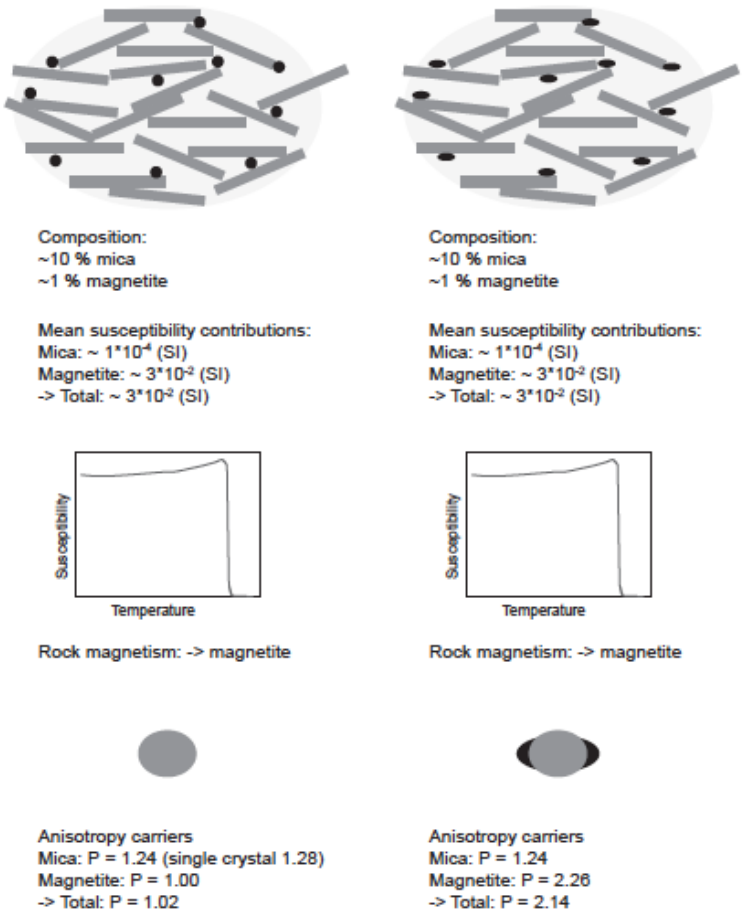

Figure 4: Relationship between carriers of bulk properties and anisotropy properties. Values reported are from calculations made using realistic properties for a 10% mica and 1% magnetite composition (note that for visual purposes the figure does not report the exact % contributions): single crystal properties for biotite, taking into account the shown orientation distribution; 20 SI intrinsic susceptibility for magnetite with shape anisotropy, assuming oblate particles. Estimates for K_{mean} from biotite crystal data (Biedermann, 2018) and Clark's (1997) relationship between magnetite vol% and K_{mean}.

ered more specifically in a following article.

Anomalous, oblique and tilted fabrics

Comparisons between magnetic and macroscopic fabrics have often resulted in classifications of "anomalous", "oblique" and "tilted" fabrics presented in the literature. Those terms were used to describe observations that did not fit the expectation of coaxial fabrics, i.e., the easy magnetization direction along the macroscopic lineation, and hard magnetization axis normal to the foliation. Through the development of anisotropy methods and modeling we have gained a greater understanding of why macroscopic and magnetic fabrics are not always parallel. Detailed characterization of single crystal magnetic properties and the ability to predict magnetic fabrics for given mineral alignments, in combination with knowledge of macroscopic mineralogical foliation and lineation, help characterize the mineral preferred orientation with more accuracy.

In amphibolites, for example, whether the maximum susceptibility is parallel or ~orthogonal to the macroscopic lineation, informs whether the amphiboles have a *c*-fiber texture (coaxial fabrics), or if their texture is a combination of *a*-fiber and point distribution (perpendicular lineations) (Biedermann et al., 2018). Therefore, additional information can be gained from a comparison between magnetic and macroscopic fabrics and/or crystal properties, allowing to determine that fabrics labeled "anomalous" in fact have a solid foundation residing in specific crystallographic properties.

Qualitative terms to describe magnetic fabric attitude, such as "oblique" or "tilted", however, are fully permissible in the absence of a specific mechanism explaining such fabrics, yet it should be understood that they may not necessarily be caused by flow/deformation conditions.

Scenarios to help interpret data

Bulk susceptibility and rock magnetic analyses can determine which minerals are present in a rock, but do not specifically inform about anisotropy carriers. The main point here is that even if magnetite dominates the bulk properties, it may or may not contribute to the anisotropy, depending on whether it has an SPO or distribution anisotropy (See Figures 1 and 4). To obtain more information on anisotropy carriers, it is therefore recommended to:

- Use HF (and/or LT) methods to separate the paramagnetic and ferromagnetic contributions to the fabric, or at least enhance the paramagnetic contribution.
- Compare the combination of K_{mean} and P, or more easily the mean deviatoric susceptibility K', observed in the rock with the single crystal properties of the constituent minerals (i.e., the maximum of these properties each mineral could contribute to the anisotropy). If no other mineral can produce a large enough K', then magnetite is a likely carrier of AMS.
- Bear in mind that a comparison of LF-AMS with AARM (or other remanence anisotropy) orientation is not sufficient, as these methods target different minerals and/or grain coercivity/size populations:
  1. Coaxiality of LF-AMS and AARM cannot be interpreted unambiguously, since a number of scenarios can lead to coaxial fabrics, e.g.:
     - Different carriers give rise to the same fabric orientation (e.g., they were aligned in the same strain field).
     - Both anisotropies are controlled by the same ferromagnetic carrier; however, "same ferromagnetic carriers" may reflect different properties with susceptibility preferentially controlled by MD magnetite, while remanence is dominated by SSD magnetite.
  2. Non-coaxiality of LF-AMS and AARM can also lead to multiple interpretations, e.g.:
     - LF-AMS is dominated by paramagnetic minerals, while AARM is dominated by ferromagnetic minerals.
     - Both could be controlled by magnetite, but in different grain size populations (MD vs

SSD, respectively) with different orientation.
- Presence of preferentially aligned SSD grains carrying inverse LF-AMS fabrics necessarily complicates interpretations further.
- Modelling of expected anisotropies for different minerals and simplified CPOs, SPOs or distributions can help understanding each mineral's contribution to the anisotropy, and the interplay of multiple anisotropy components.

Because there are many established techniques to characterize magnetic fabrics, each targeting different mineral groups in the same rock, it is important to carefully choose a suitable method for the aim of each specific study. For example, for correcting paleomagnetic data, remanence anisotropy is more appropriate compared to LF-AMS as it measures the same quantity (i.e., typically magnetization in Am^2/kg), and targets the remanence carriers. On the other hand, if the alignment of the bulk rock-forming minerals is of interest, the diamagnetic or paramagnetic component isolated, e.g., from HF-AMS, will be the most adequate.

We hope that the overview provided in this article will aid choosing a suitable technique for each study and avoid common misinterpretations.

References

Balsley, J. R., & Buddington, A. F. (1960). Magnetic susceptibility anisotropy and fabric of some Adirondack granites and orthogneisses. American Journal of Science, 258A, 6–20.

Biedermann, A. R. (2018). Magnetic Anisotropy in Single Crystals: A Review. Geosciences, 8(8), 302. https://doi.org/10.3390/geosciences8080302

Biedermann, A. R., Kunze, K., & Hirt, A. M. (2018). Interpreting magnetic fabrics in amphibole-bearing rocks. Tectonophysics, 722(November 2017), 566–576. https://doi.org/10.1016/j.tecto.2017.11.033

Borradaile, G. J. (1987). Anisotropy of magnetic susceptibility: rock composition versus strain. Tectonophysics, 138, 327–329.

Borradaile, G. J., & Henry, B. (1997). Tectonic applications of magnetic susceptibility and its anisotropy. Earth-Science Reviews, 42(1–2), 49–93. https://doi.org/10.1016/S0012-8252(96)00044-X

Borradaile, G. J., & Jackson, M. J. (2010). Structural geology, petrofabrics and magnetic fabrics (AMS, AARM, AIRM). Journal of Structural Geology, 32(10), 1519–1551. https://doi.org/10.1016/j.jsg.2009.09.006

Bowles, J., Jackson, M. J., & Banerjee, S. K. (2010). Interpretation of Low-Temperature Data Part II: The Hematite Morin Transition. Institute for Rock Magnetism, 20(1), 1–11. Retrieved from http://www.irm.umn.edu/quarterly/irmq20-1.pdf

Cañón-Tapia, E. (1996). Single-grain versus distribution anisotropy: a simple three-dimensional model. Physics of the Earth and Planetary Interiors, 94(1–2), 149–158. https://doi.org/10.1016/0031-9201(95)03072-7

Cañón-Tapia, E. (2001). Factors affecting the relative importance of shape and distribution anisotropy in rocks: theory and experiments. Tectonophysics, 340(1–2), 117–131. https://doi.org/10.1016/S0040-1951(01)00150-0

Clark, D. A. (1997). Magnetic petrophysics and magnetic petrology: aids to geological interpretation of magnetic surveys. Journal of Australian Geology and Geophysics, 17, 83–103.

Elhanati, D., Issachar, R., Levi, T., & Weinberger, R. (2021). A Practical Approach for Identification of Magnetic Fabric Carriers in Rocks. Journal of Geophysical Research: Solid Earth, 126(5). https://doi.org/10.1029/2020JB021105

Finke, W. (1909). Magnetische Messungen an Platinmetallen und monoklinen Kristallen, insbesondere der Eisen-, Kobalt- und Nickelsalze. Annalen Der Physik, 336(1), 149–168.

Hargraves, R. B., Johnson, D., & Chan, C. Y. (1991). Distribution anisotropy: The cause of AMS in igneous rocks? Geophysical Research Letters, 18(12), 2193–2196. https://doi.org/10.1029/91GL01777

Housen, B. A., & van der Pluijm, B. A. (1990). Chlorite control of correlations between strain and anisotropy of magnetic susceptibility. Physics of the Earth and Planetary Interiors, 61, 315–323.

Issachar, R., Levi, T., Lyakhovsky, V., Marco, S., & Weinberger, R. (2016). Improving the method of low-temperature anisotropy of magnetic susceptibility (LT-AMS) measurements in air. Geochemistry, Geophysics, Geosystems, 17(7), 2940–2950. https://doi.org/10.1002/2016GC006339

Issachar, R., Levi, T., Marco, S., & Weinberger, R. (2018). Separation of Diamagnetic and Paramagnetic Fabrics Reveals Strain Directions in Carbonate Rocks. Journal of Geophysical Research: Solid Earth, 123(3), 2035–2048. https://doi.org/10.1002/2017JB014823

Jackson, M. J., Moskowitz, B., & Bowles, J. (2011). Interpretation of Low-Temperature Data Part III: The Magnetite Verwey Transition (Part A). The IRM Quarterly, 20(4), 1–11.

Jelinek, V. (1984). On a mixed quadratic invariant of the magnetic susceptibility tensor. Journal of Geophysics - Zeitschrift Fur Geophysik, 56(1), 58–60.

Kligfield, R., Lowrie, W., & Dalziel, I. W. D. (1977). Magnetic susceptibility anisotropy as a strain indicator in the sudbury basin, Ontario. Tectonophysics, 40(3–4), 287–308. https://doi.org/10.1016/0040-1951(77)90070-1

König, W. (1887). Magnetische Untersuchungen an Krystallen. Annalen Der Physik, 267(6), 273–302.

Osborn, J. A. (1945). Demagnetizing Factors of the General Ellipsoid. Physical Review, 67(11–12), 351–357. https://doi.org/10.1103/PhysRev.67.351

Parés, J. M., & van der Pluijm, B. A. (2002). Phyllosilicate fabric characterization by Low-Temperature Anisotropy of Magnetic Susceptibility (LT-AMS). Geophysical Research Letters, 29(24), 68-1-68–4. https://doi.org/10.1029/2002GL015459

Potter D. K., & Stephenson, A. (1988). Single-domain particles in rocks and magnetic fabric analysis. Geophysical Research Letters 15(10): 1097–1100.

Rochette, P., Aubourg, C., & Perrin, M. (1999). Is this magnetic fabric normal? A review and case studies in volcanic formations. Tectonophysics, 307(1–2), 219–234. https://doi.org/10.1016/S0040-1951(99)00127-4

Schmidt, V., Hirt, A. M., Rosselli, P., & Martín-Hernández, F. (2007). Separation of diamagnetic and paramagnetic anisotropy by high-field, low-temperature torque measurements. Geophysical Journal International, 168(1), 40–47. https://doi.org/10.1111/j.1365-246X.2006.03202.x

Stenger, F. (1888). Ueber die Gesetze des Krystallmagnetismus. Annalen Der Physik Und Chemie, 271(10), 331–353. https://doi.org/10.1002/andp.18882711008

Stoner, E. C. (1945). XCVII. The demagnetizing factors for

ellipsoids. The London, Edinburgh, and Dublin Philosophical Magazine and Journal of Science, 36(263), 803–821. https://doi.org/10.1080/14786444508521510

Tarling, D. H., & Hrouda, F. (1993). The Magnetic Anisotropy of Rocks (p. 217 pp.). London: Chapman and Hall.

Tyndall, J. (1851). Ueber Diamagnetismus und magnekrystallinische Wirkung. Annalen Der Physik, 159(7), 384–416.

The IRM Quarterly

The *Institute for Rock Magnetism* is dedicated to providing state-of-the-art facilities and technical expertise free of charge to any interested researcher who applies and is accepted as a Visiting Fellow. Short proposals are accepted semi-annually in spring and fall for work to be done in a 10-day period during the following half year. Shorter, less formal visits are arranged on an individual basis through the Facilities Manager.

The *IRM* staff consists of **Subir Banerjee**, Emeritus Professor/Founding Director; **Bruce Moskowitz**, Professor/Director; **Joshua Feinberg**, Associate Professor/Associate Director; **Maxwell Brown,** Facility Manager; **Peat Sølheid,** Senior Staff Scientist**; Dario Bilardello**, Associate Research Professor.

Funding for the *IRM* is provided by the **National Science Foundation**, the **W. M. Keck Foundation**, and the **University of Minnesota**.

UNIVERSITY OF MINNESOTA

The *IRM Quarterly* is published four times a year by the staff of the *IRM*. If you or someone you know would like to be on our mailing list, if you have something you would like to contribute (*e.g.*, titles plus abstracts of papers in press), or if you have any suggestions to improve the newsletter, please notify the editor:

Dario Bilardello
Institute for Rock Magnetism
University of Minnesota
150 John T Tate Hall
116 Church Street SE
Minneapolis, MN 55455-0128
phone: (612) 624-5049
e-mail: dario@umn.edu
www.irm.umn.edu